SANDIA REPORT

SAND2003-1980
Unlimited Release
Printed June 2003

Multi- and Hyper-Spectral Sensing for Autonomous Ground Vehicle Navigation

R. Joseph Fogler

Prepared by
Sandia National Laboratories
Albuquerque, New Mexico 87185 and Livermore, California 94550

Sandia is a multiprogram laboratory operated by Sandia Corporation,
a Lockheed Martin Company, for the United States Department of Energy under Contract DE-AC04-94AL85000.

Issued by Sandia National Laboratories, operated for the United States Department of Energy by Sandia Corporation.

Available to DOE and DOE contractors from
U.S. Department of Energy
Office of Scientific and Technical Information
P.O. Box 62
Oak Ridge, TN 37831

Telephone: (865)576-8401
Facsimile: (865)576-5728
E-Mail: reports@adonis.osti.gov
Online ordering: http://www.doe.gov/bridge

Available to the public from
U.S. Department of Commerce
National Technical Information Service
5285 Port Royal Rd
Springfield, VA 22161

Telephone: (800)553-6847
Facsimile: (703)605-6900
E-Mail: orders@ntis.fedworld.gov
Online order: http://www.ntis.gov/help/ordermethods.asp?loc=7-4-0#online

SAND2003-1980
Unlimited Release
Printed June 2003

Multi- and Hyper-Spectral Sensing for Autonomous Ground Vehicle Navigation

R. Joseph Fogler
Signal & Image Processing Systems
Sandia National Laboratories
P. O. Box 5800
Albuquerque, NM 87185-0844

Abstract

Robotic vehicles that navigate autonomously are hindered by unnecessary avoidance of soft obstacles, and entrapment by potentially avoidable obstacles. Existing sensing technologies fail to reliably distinguish hard obstacles from soft obstacles, as well as impassable thickets and other sources of entrapment. Automated materials classification through advanced sensing methods may provide a means to identify such obstacles, and from their identity, to determine whether they must be avoided.

Multi- and hyper-spectral electro-optic sensors are used in remote sensing applications to classify both man-made and naturally occurring materials on the earth's surface by their reflectance spectra. The applicability of this sensing technology to obstacle identification for autonomous ground vehicle navigation is the focus of this report. The analysis is restricted to system concepts in which the multi- or hyper-spectral sensor is on-board the ground vehicle, facing forward to detect and classify obstacles ahead of the vehicle. Obstacles of interest include various types of vegetation, rocks, soils, minerals, and selected man-made materials such as paving asphalt and concrete.

This work was sponsored by Lockheed-Martin Missile and Fire Control, under shared vision agreement number SC99/01573 for Ground Autonomy Platform Enabler (GAPE) technology.

Acknowledgments

The author would like to thank Jody L. Smith for providing keen insights and a wealth of information on reflectance spectroscopy and atmospheric effects. I would also like to thank Jody for designing and conducting simulation runs for obtaining atmospheric transmittance spectra, and providing reflectance databases for my experiments. I would also like to thank Mary M. Moya for providing literature references and helping to craft the statement of work.

Table of Contents

Nomenclature

VIS	visible (i.e. visible spectrum)
NIR	near infrared
SWIR	short-wave infrared
MWIR	medium-wave infrared
LWIR	long-wave infrared
CCD	charge coupled device
CIR	color-infrared
NDI	normalized difference index
NDVI	normalized difference vegetation index
ROC	receiver operating characteristic
Si	silicon
InGaAs	Indium Gallium Arsenide
InSb	Indium Lead
FOV	field of view
LED	light emitting diode
6S	*Second Simulation of Satellite Signal in the Solar Spectrum* atmospheric simulation software code

Introduction

This report documents efforts conducted under a Sandia National Laboratories and Lockheed-Martin Company joint vision project for improving autonomous ground vehicle navigation. Autonomous ground vehicles that utilize existing sensing technologies such as video cameras, laser radars, or tactile sensors for navigation are hindered by unnecessary avoidance of soft obstacles, and entrapment by potentially avoidable obstacles. Existing sensing technologies fail to reliably distinguish hard obstacles from soft obstacles, as well as impassable thickets and other sources of entrapment. Materials classification may provide a means to identify such obstacles, and from their identity, to determine whether they must be avoided.

Multi- and hyper-spectral electro-optic sensors are used in remote sensing applications to classify both man-made and naturally occurring materials on the earth's surface by their reflectance spectra. The applicability of this sensing technology to obstacle identification for autonomous ground vehicle navigation is the focus of this report. The analysis is restricted to system concepts in which the multi- or hyper-spectral sensor is on-board the ground vehicle, facing forward to detect and classify obstacles ahead of the vehicle. Obstacles of interest include various types of vegetation, rocks, soils, minerals, and a few man-made materials such as paving asphalt and concrete.

Spectral Bands for Remote Sensing

The primary regions of the Electro-Magnetic (EM) spectrum used by electro-optic sensors for earth remote sensing are shown in Table 1 [1]. The wavelength bands are determined by atmospheric windows, which are bracketed by regions of low atmospheric transmittance due to absorption by atmospheric gases. Small variations in the band ranges can be found in different references because the boundaries of some atmospheric windows are not distinct.

Table 1. The primary spectral bands used in earth remote sensing.

Band name	Wavelength range	Radiation source	Surface property of interest
Visible (VIS)	0.4 – 0.7 μm	Solar	Reflectance
Near InfraRed (NIR)	0.7 – 1.1 μm	Solar	Reflectance
Short Wave InfraRed (SWIR)	1.1 – 1.35 μm 1.4 – 1.8 μm 2 – 2.5 μm	Solar	Reflectance
Mid Wave InfraRed (MWIR)	3 – 4 μm 4.5 – 5 μm	Solar, Thermal	Reflectance, Temperature
Thermal InfraRed (TIR)	8 – 9.5 μm 10 – 14 μm	Thermal	Temperature

All materials with temperatures above absolute zero (0^oK) emit thermal radiation. An ideal blackbody emits thermal radiation according to Planck's blackbody equation. In general, most materials are graybodies whose emission spectra are those of a blackbody modified by a wavelength-dependent emissivity function. In daylight, materials also reflect solar radiation in a wavelength-dependent fashion. The reflectance spectrum of a material depends upon its chemical properties and physical structure, and the spectrum of the illuminant.

All materials passively absorb and reflect solar radiation in the visible (VIS) through short wave infrared (SWIR) bands. In daylight, reflected radiation from materials on the earth's surface in these bands is substantially stronger than self-emitted radiation from the same materials due to their absolute temperature. Conversely, in the thermal infrared (TIR) band, self-emitted radiation is substantially stronger than reflectance. Thus, in the VIS through SWIR bands, the property of interest is primarily reflectance, whereas, in the TIR band, the property of interest is temperature arising from self-emission. In the mid wave infrared (MWIR) band, reflected and emitted radiation exhibit roughly equal strength from surface materials and are difficult to unmix.

Emissivity functions must provide distinctive signatures in order to be useful for the identification of materials by self-emission. Unfortunately, a plant leaf can exhibit hundreds of different emissivity functions across its surface [2]. Thus, the spectral character of emitted radiation is too variable for the identification of vegetation types. This means that the TIR band is of little use in the materials identification problem.

The reflectance spectrum of a material is a function of the spectral characteristics of the illuminant modified by the surface properties and molecular structure of the material. The chemical constituents and molecular bonds that bind them create absorption features that form a unique spectral signature. The illuminant must be characterized, however, in order to discount its contribution to the overall spectral shape.

In remote sensing, solar radiation modified by atmospheric absorption is the source of illumination. Identification of materials on the earth's surface is conducted primarily in the VIS through SWIR (0.4μm through 2.5μm) bands. The MWIR bands are primarily used for analyzing atmospheric gases.

Solar Exitance and Atmospheric Transmittance

Direct solar radiation received above the earth's atmosphere has a constant and known spectral content. A *Second Simulation of Satellite Signal in the Solar Spectrum (6S)* atmospheric modeling code simulation in the visible through short-wave bands is shown in Figure 1. The solar irradiation spectrum peaks at around 0.5μm in the figure and decreases monotonically with increasing wavelength [3].

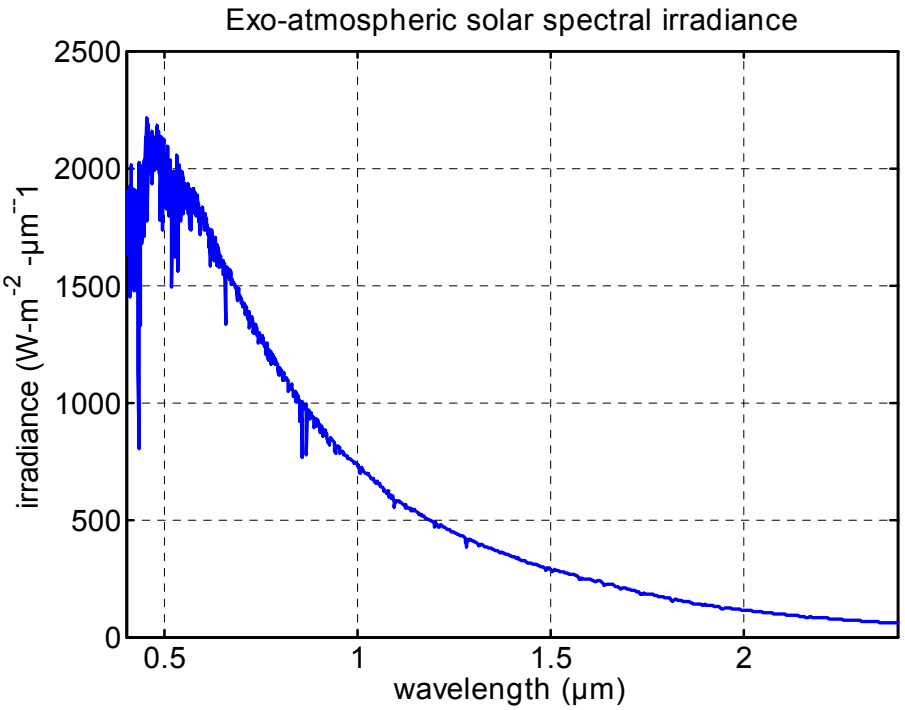

Figure 1. 6S modeling software simulation of exo-atmospheric solar spectral irradiance.

The solar spectrum observed at ground level is modified by atmospheric absorption and scattering. The fraction that arrives at a location on earth is called the *solar path transmittance*, $\tau_s(\lambda)$, which is a strong function of wavelength. An example of direct solar radiation seen at the earth's surface in a desert region with low concentrations of atmospheric aerosols is simulated in Figure 2. The molecular absorption bands of atmospheric H_2O and CO_2 cause deep absorption features that can be seen in the figure. Two bands near 1.4µm and 1.9µm can completely block the transmission of radiation. The absence of transmittance in these regions precludes their use in obtaining reflectance information and those wavelengths. Other H_2O absorption bands near 0.9µm and 1.1µm are narrower and less deep. These regions yield reflectance values that are strongly dependent on the amount of water vapor in the atmosphere.

The observant reader may note that the transmittance curve in Figure 2 lacks the convex upward shape (i.e. curving downward at the wavelength extremes) often seen in textbooks. The difference here is due to the lower concentration of atmospheric aerosols characteristic of desert regions.

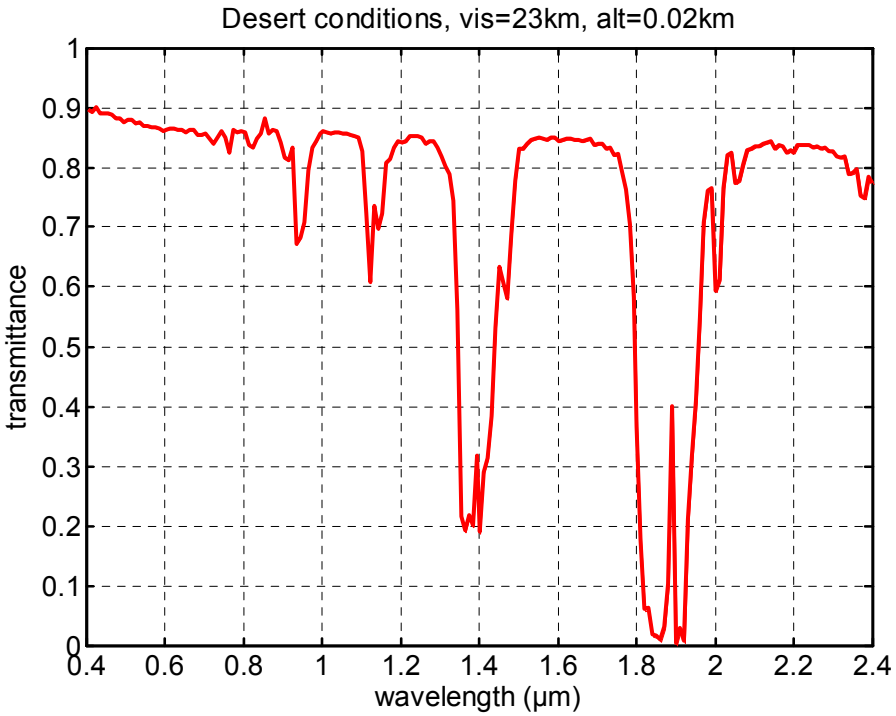

Figure 2. 6S simulation of atmospheric transmittance in the VIS through SWIR spectral bands for a desert region with low atmospheric aerosols.

Solar radiation is also received on the ground indirectly through *skylight* radiation, which is scattered downward by the atmosphere. Skylight radiation is the reason that shadows seen on the earth's surface are not completely black.

The spectral reflectance of plants and other materials found at the earth's surface can be characterized under laboratory conditions. However, the observed reflectance when illuminated by solar irradiation under the influence of the atmosphere and clouds will yield substantial variations in spectral shape compared to the laboratory model. Thus, materials identification strategies employed in remote sensing must either be inherently insensitive to spectral variations due to atmospheric effects, or the atmospheric effects must be measured and removed from the reflectance measurements in order to obtain consistent signatures. Features within these reflectance signatures must ultimately be relatable to those observed in laboratory data.

Reflectance Spectra Databases and Material Classes

A number of spectral libraries are available in the open literature. The primary emphasis of many of these libraries is geological. As such, they contain laboratory spectra for a variety of soils, rocks and minerals. A few spectral libraries contain laboratory spectra for materials such as vegetation, water, and man-made materials.

The following spectral libraries were utilized for obtaining the results presented in this report:

- U.S. Geological Survey (USGS) vegetation spectral library [5]
- Published Dry Plant Material Spectra (PDPMS) library [6]
- Jasper Ridge Spectral Library (JRSL) library for green vegetation, dry vegetation, and rocks
- USGS mineral spectral library [5]
- Jet Propulsion Laboratory (JPL) mineral spectral libraries [7]
- John Hopkins University (JHU) spectral library [8-11]
- Nonconventional Exploitation Factors Data System (NEFDS) 9.1 spectral library [12]

The range and spacing of wavelengths over which the library measurements were taken differed among the databases. The data of interest for this report were those that spanned the 0.4μm to 2.4μm wavelength range with measurements at 0.1μm spacing. The fine spacing was needed to match the wavelength resolution of modern hyperspectral sensors. Linear interpolation was used to construct data at the desired wavelengths when laboratory measurements were finer than 0.01μm but straddled the desired wavelengths. Those library instances that lacked data in the desired wavelengths were removed from consideration.

The remaining data were then grouped into seven materials classes – vegetation, soils, rocks, minerals, man-made materials, water, and chemical constituents of plant materials. The materials classes, number of instances in each class, and the spectral libraries from which the instances were drawn, are listed in Table 2. The short (five-letter) tag names listed in the table were assigned to each class for convenience.

Table 2. Material classes and the databases from which material instances were drawn. The codes are five-letter shorthand names for the material classes.

Material Class	Tag	Instances	Spectral Libraries
Vegetation	`flora`	97	USGS vegetation, PDPMS, JRSL
Soils	`soils`	25	JHU
Rocks	`rocks`	135	JHU
Minerals	`miner`	479	USGS minerals
Man-made materials	`mmade`	29	JHU, NEFDS
Water	`water`	9	USGS minerals, JHU, NEFDS
Chemical constituents	`chems`	15	PDPMS

The chemical constituents materials class contains substances extracted from plant material such as cellulose and lignin that exhibit reflectance spectra indicative of plant chemistry. They would not be expected to exist in isolation under remote sensing

conditions. Thus, they are useful for analytical purposes but not as exemplars for materials discrimination.

Problem Wavelengths Due to Atmosphere

It is important to consider that library reflectance spectra do not include the effects of atmospheric transmittance. Although there might be a unique spectral feature in the library reflectance spectrum of a particular material, if that feature occurs at wavelength where there is substantial attenuation due to atmospheric absorption, the feature will either be too weak to be measured, or simply unreliable due to high variability with atmospheric conditions. Potentially problematic atmospheric absorption feature wavelengths in the 0.4µm to 2.4µm range are listed in Table 3. Values in the table are rounded to the nearest 0.1µm for convenience.

Oxygen absorbs at 0.76µm in a narrow feature and carbon dioxide absorbs at 2.01µm and 2.06µm, plus a weak doublet near 1.6µm. Water causes most of the remaining absorption features throughout the spectrum and hides additional weaker absorptions from other gases [4]. The first of two wide-and-deep water absorption features occur approximately in the region 1.31µm to 1.50µm, which is shaded gray in the table. The second occurs in the region 1.75µm to 2.06µm, which is shaded in light blue. These absorption feature regions have wide bottoms and sharply sloping edges. The bottom regions and adjacent edge regions are delineated in the table. A third feature region begins at approximately 2.35µm and slopes downward in reflectance toward 2.4µm. The exact boundaries of the wide absorption regions are arguable. They depend on how far down the sloping edges of the broad absorption regions one chooses to establish them. Thus, the wavelength ranges of the broad absorption features should only be considered approximations.

Table 3. Atmospheric absorption feature wavelengths in the 0.4µm to 2.4µm range.

Wavelength (µm)	Band	Absorption features	Shape	Depth
0.72	NIR	CO_2	Narrow	Shallow
0.76	NIR	O_2	Narrow	Moderate
0.81	NIR	CO_2	Narrow	Shallow
0.94-0.97	NIR	H_2O	Moderate	Moderate
1.13-1.17	SWIR I	H_2O	Moderate	Moderate
1.31-1.35	SWIR I	H_2O, CO_2	Edge	Border Deep
1.36-1.39	-	H_2O, CO_2	Broad	Deep
1.40-1.50	SWIR II	H_2O, CO_2	Edge	Border Deep
1.6	SWIR II	CO2	Doublet	Shallow
1.75-1.80	SWIR II	H_2O, CO_2	Broad	Border Deep
1.81-1.94	-	H_2O, CO_2	Broad	Deep
1.95-2.00	-	H_2O, CO_2	Broad	Border Deep
2.01	SWIR III	CO_2	Narrow	Border Deep
2.02-2.05	SWIR III	H_2O	Edge	Border Deep
2.06	SWIR III	CO_2	Narrow	Border Deep
2.35-2.40	SWIR III	H_2O	Edge	Border Deep

Wavelength ranges that represent deep absorption features in the table, may yield reflectance values that are too small to measure. Wavelengths that border deep absorption troughs have high variability and are difficult to utilize in an absolute sense. However, they can be of some use in relative comparisons of absorption levels in pixel neighborhoods within a given scene. Wavelengths that have shallow features can be used cautiously if measurements are averaged over broad wavelength windows.

Spectral Features of Material Classes

In this section, we examine the reflectance spectra of selected instances from each of the materials classes. Features of the reflectance spectra that may be useful for distinguishing between materials classes by remote sensing are described, as well as the underlying chemistry and physics from which they arise.

Soils

A typical laboratory reflectance spectrum for soils is shown in Figure 3. Soil spectra have very few distinguishing features. There is a gentle rise in reflectance from 0.4µm to about 1.3µm, and absorption features occur at 1.4µm, 1.9µm, and 2.2µm. The shallow absorption feature at 1.4µm and the deeper feature at 1.9µm are due to water absorption and are generally less pronounced than those occurring in vegetation reflectance spectra. The first of these two features can be utilized in a relative sense to help distinguish soils from vegetation, provided that there is a measurable amount of reflectance available at this wavelength. The second feature wavelength is unlikely to be measurable due to stronger atmospheric attenuation, as indicated in Figure 2.

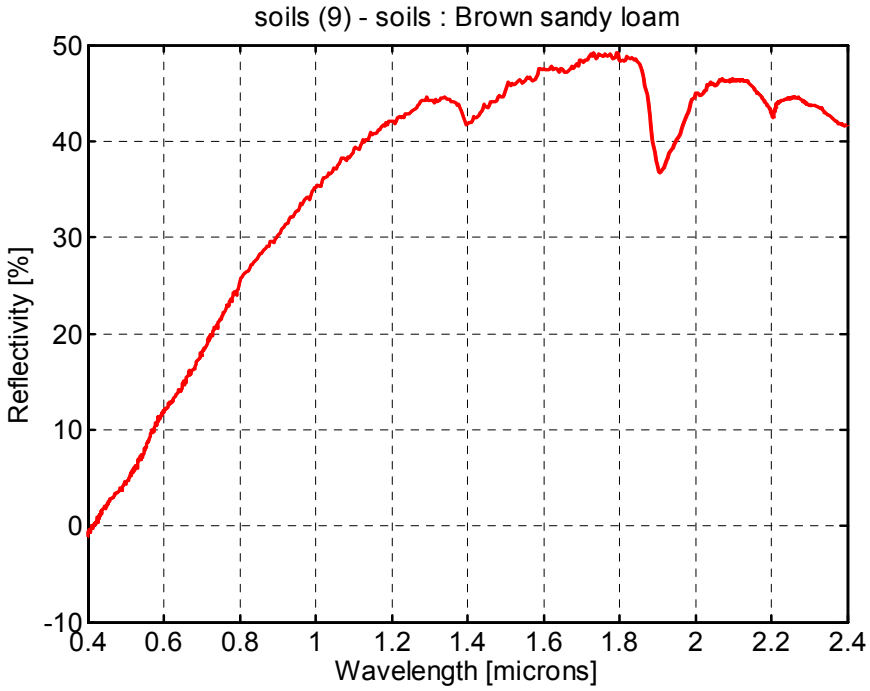

Figure 3. Laboratory reflectance spectrum of a brown, sandy loam soil.

The most unique soil feature occurs at 2.2µm. This feature is due to the absorption properties of clay minerals within the soil such as Kaolinite, Montmorillonite, and Muscovite [4]. This feature is probably the best discriminator for separating soils from dry vegetation, rocks and some minerals. However, if the clay minerals exist in low concentrations in the soil, or the soil is exceptionally gravelly, the feature may not be detectable.

Vegetation

The reflectance spectrum of a green lawn grass from the USGS vegetation spectral library is shown in Figure 4. A number of features can be seen that are typical of the reflectance spectra of photosynthetic (green and wet) vegetation. Reflectance in the visible part of the spectrum is low even though solar irradiance is maximal in that wavelength region. Reflectance is high in the NIR region with a very rapid transition between the red and NIR regions at approximately 0.7µm. This feature is called the *red edge*, and is highly unique compared to what is observed in the reflectance spectra of other materials such as soils, rocks and minerals.

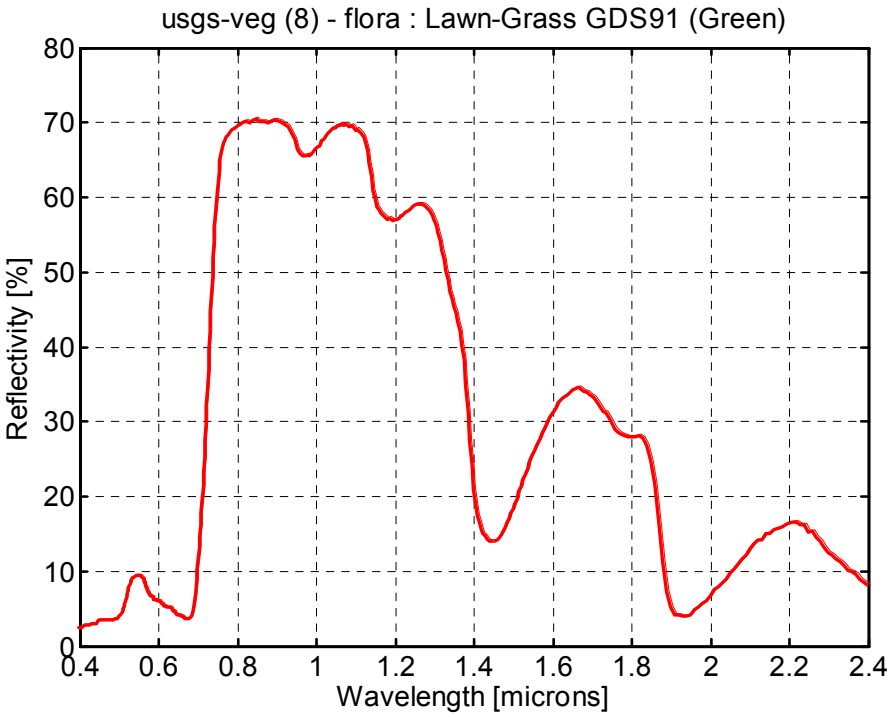

Figure 4. Laboratory reflectance spectrum of green lawn grass, exhibiting the typical character of photosynthetic (green and wet) vegetation.

Reflectance peaks in the NIR band, generally centered at 0.8µm and 1.25µm, are referred to as the infrared plateau. High reflectance in this area is caused by strong scattering from plant cell walls, and contains diagnostic information based on the cellular arrangement of the tissue as well as in the hydration state of the leaf.

Chlorophyll absorption features occur around 0.48µm in the blue visible region, and 0.675µm in the red visible region, and are a function of electronic transitions in the cartenoid pigments associated with the photosynthetic process [13]. Additional absorption features occur at 0.58µm, in the yellow visible region, and at 0.61µm, in the orange visible region, due to protochlorophyll, and chlorophyll-b, respectively. Between these two absorption regions a small plateau can be seen in the green visible region from 0.53µm to 0.56µm.

The library reflectance spectra for a green lawn grass, dry grass, and sandy loam soil are shown in Figure 5. The lawn grass and soil spectra are the same as those in Figure 4 and Figure 3, respectively. The dry grass spectrum (shown in red) is characteristic of nonphotosynthetic vegetation. Note the absence of chlorophyll absorption features in the visible region of the spectrum, and the relative weakness of the red edge feature compared to the green lawn grass (shown in green).

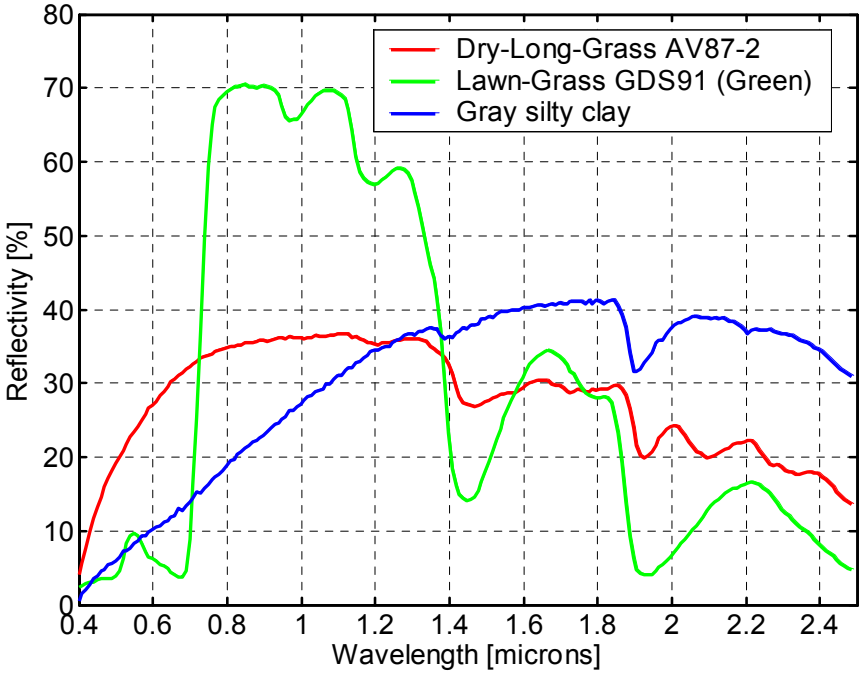

Figure 5. Laboratory reflectance spectrum of a green lawn grass, dry grass, and sandy loam soil.

The loss of chlorophyll absorption in the visible region and weakened red edge are characteristic of the reflectance spectra of senesced leaves of deciduous species. As a leaf begins to senesce, chlorophyll absorption decreases. With further senescence, both chlorophyll absorption and the red edge become week. Dead leaves exhibit no chlorophyll absorption feature at all. Thus, vegetation can exhibit a continuum of spectral shapes in the visible and NIR regions. This makes vegetation a difficult material class to 1) consolidate into a single monolithic material class, and to 2) separate that class from other material classes, given only the chlorophyll absorption and red edge features.

Evergreen trees and shrubs retain strong chlorophyll absorption and red edge features year round. Thus, this subset of the vegetation class can be easily and consistently separated from non-vegetation classes. Some deciduous vegetation can be separated in the same manner, but only seasonally.

Since the chlorophyll absorption features in the visible spectrum, and the red edge feature are inadequate for distinguishing nonphotosynthetic vegetation from other material classes, we must seek features at higher wavelengths. Liquid water in leaves is the most important absorber beyond 1µm, but several plant materials have significant absorptions between 1µm and 2.4µm. These latter absorptions represent important features for discriminating nonphotosynthetic vegetation.

The strongest absorption features in nonphotosynthetic vegetation beyond 1µm, excluding water absorption, come from the plant substance cellulose, and to a lesser extent, lignin and nitrogen [14]. Examples of reflectance spectra for plant cellulose and lignin are shown in Figure 6. Several absorption features are visible in the figure. Absorption wavelengths that have been associated with these substances are listed in Table 4.

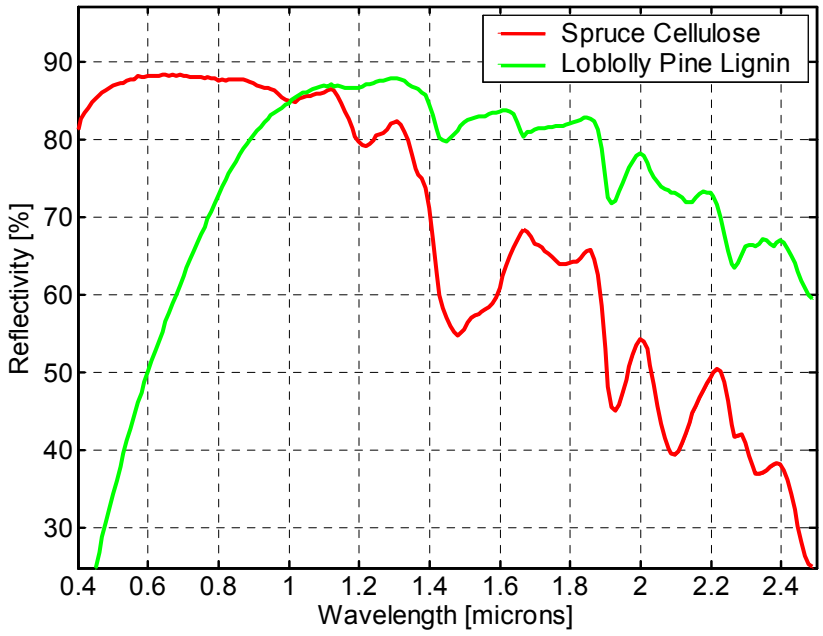

Figure 6. Reflectance spectra for spruce cellulose and loblolly pine lignin.

Table 4. Substances that exhibit useful absorption features in dry vegetation.

Substance	**Wavelength (microns)**
Cellulose	*1.48, 1.93*, **2.10, 2.28, 2.34**, *2.48*
Lignin	*1.45,* **1.68**, *1.93*, **2.04 to 2.14, 2.27, 2.33**, *2.38, 2.50*
Nitrogen	**0.99, 1.12**, *1.46*, **1.66**, *1.93*, **2.13, 2.26, 2.32**, *2.50*

Wavelengths that do not fall within strong atmospheric absorption bands are listed in bold font in the table. These wavelengths are suitable candidates for distinguishing plant species, and for separating dry, nonphotosynthetic vegetation from other material classes. The methodology for exploiting these feature wavelengths is presented in a later section.

Minerals

The processes that produce absorption bands in the spectra of materials are rather complex. The underlying physics of these processes are described in this section, which draws extensively from reference [4].

Absorption Band Processes

There are two general processes that cause absorption bands in the spectra of materials -- electronic and vibrational.

Electronic Processes

The most common electronic process revealed in mineral spectra is due to unfilled electron shells of transition elements such as nickel, chromium, cobalt, and iron. Iron is the most common transition element found in minerals. Isolated ions of transition elements have identical *d*-orbital energies but when the atoms are located in a crystal field, the energy levels split. The crystal field varies with crystal structure from mineral to mineral and thus the amount of splitting varies. This makes specific mineral identification possible from spectroscopy.

Absorptions can also be caused by charge transfers where the absorption of a photon causes an electron to move between ions, or between ions and ligands. These absorptions are hundreds to thousands of times stronger than crystal field transitions. Charge transfer absorptions are the main cause of the red color of iron oxides and hydroxides. Reflectance spectra of iron oxides have such strong absorption bands that the shape changes significantly with grain size.

In some minerals, there are two energy levels in which electrons may reside – the *conduction band*, where electrons move freely throughout the lattice, and a lower energy *valence band*, where electrons are attached to individual atoms. The difference between the two energy levels is called the band gap. The band gap is typically small or non-existent in metals, and very large in dielectrics. In semiconductors, the band gap corresponds to the energy of visible to near-infrared wavelength photons and the their spectra approximate a step function. The yellow color of sulfur is caused by such a band gap.

A few minerals show color due to absorption by *color centers*. Color centers are caused by illumination of crystal imperfections and impurities. The yellow, purple, and blue colors of fluorite are caused by color centers.

Vibrational Processes

The bonds in a molecule or crystal lattice can be likened to a vibrating mechanical system of springs with attached weights. The frequency of vibration depends on the strength of the bond in a molecule (the springs) and the mass of each element in a molecule (the weights). For a molecule with N atoms, there are 3N-6 normal modes of vibrations called fundamentals. Each vibration can also occur at roughly multiples of a fundamental frequency. Thus, reflectance spectra of minerals can be quite complex.

The additional vibrations are called overtones when they involve multiples of a single fundamental mode, and combinations when they involve different modes of vibration. Each higher overtone or combination is typically 30 to 100 times weaker than the last. In reflectance spectroscopy, these weak absorptions can be measured and diagnostic information routinely gained from 2nd and 3rd overtones and combinations.

Sample Mineral Spectra

Laboratory reflectance spectra for samples of the minerals Alunite, Beryl, and Calcite are shown in Figure 7. The three shallow absorption features at 1.88µm, 1.99µm and 2.16µm, and the deep absorption feature at 2.34µm in the Calcite sample are vibrational bands due to CO_3. The Alunite sample exhibits shallow absorption features at 1µm and 1.27µm that represent vibrational bands due to OH and Al-OH, respectively. The pair of deep absorption features at 1.44µm and 1.49µm is due to OH. The deep absorption feature at 1.77µm, and two additional features at 2.17µm and 2.32µm are due to Al-OH.

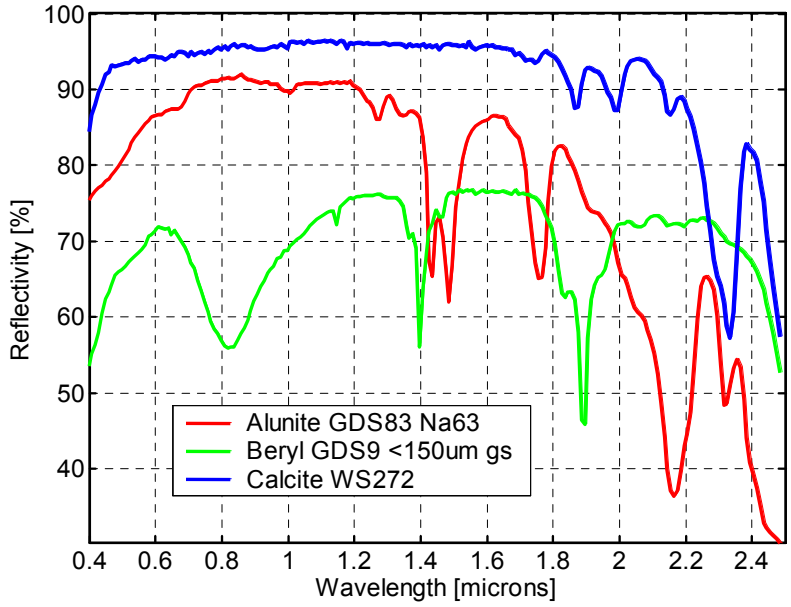

Figure 7. Laboratory reflectance spectra for some selected minerals.

The wide dip at 0.82µm in the Beryl reflectance spectrum is due to Fe^{2+} iron crystal field absorption. The deep dips at 1.4µm and 1.9µm arise from vibrational bands due to water [4].

A cursory examination of the reflectance spectra in Figure 7 indicates that 1) the absorption feature at 1.99μm is diagnostic of Calcite, 2) the absorption features at 1.49μm and 1.77μm is diagnostic of Alunite, and 3) the absorption feature at 0.82μm is diagnostic of Beryl, separating each from the other two minerals. This is a simplistic example of reflectance spectroscopy for mineral identification, but it captures the general strategy.

Rocks

Rocks are commonly divided into three major classes according to the processes that resulted in their formation. These classes are igneous, sedimentary, and metamorphic.

Igneous rocks are any of a variety of glassy rocks formed by the cooling and solidification of molten earth material. A great majority of igneous rocks are composed of silicate materials such as pyroxene, amphibole, olivine, and mica. Minor occurrences of carbon-rich igneous rocks, e.g. containing sodium carbonate but low in silicates, have been found.

The bonding of sediments from broken down minerals creates sedimentary rocks. There are two principle types – detrital and authigenic. Detrital rock is formed by the accumulation and lithification of sediment composed of grains of minerals such as quartz and feldspar that may have been transported to the depositional site. Authigenic rock is formed from minerals such as calcite, halite and gypsum within the depositional site in response to geochemical processes.

Metamorphic rocks are formed by the alteration of preexisting rocks in response to changing environmental conditions such as temperature, pressure, mechanical stress, and the addition or removal of chemical components. Metamorphic rocks may be formed from igneous, sedimentary, or other preexisting metamorphic rocks.

Laboratory reflectance spectra for examples from each of the three major rock classes are shown in Figure 8, Figure 9, and Figure 10. Since rocks are composed of minerals, the same strategies employed for mineral identification via reflectance spectroscopy are applicable to the identification of rocks.

The metamorphic rock sample -- Chloritic Gneiss – shown in Figure 10, is particularly intriguing. Its reflectance spectrum contains features that mimic the chlorophyll absorption and the red edge features in the visible and NIR wavelengths observed for photosynthetic vegetation. As such, it would take very careful spectral analysis to distinguish this particular metamorphic rock type from vegetation.

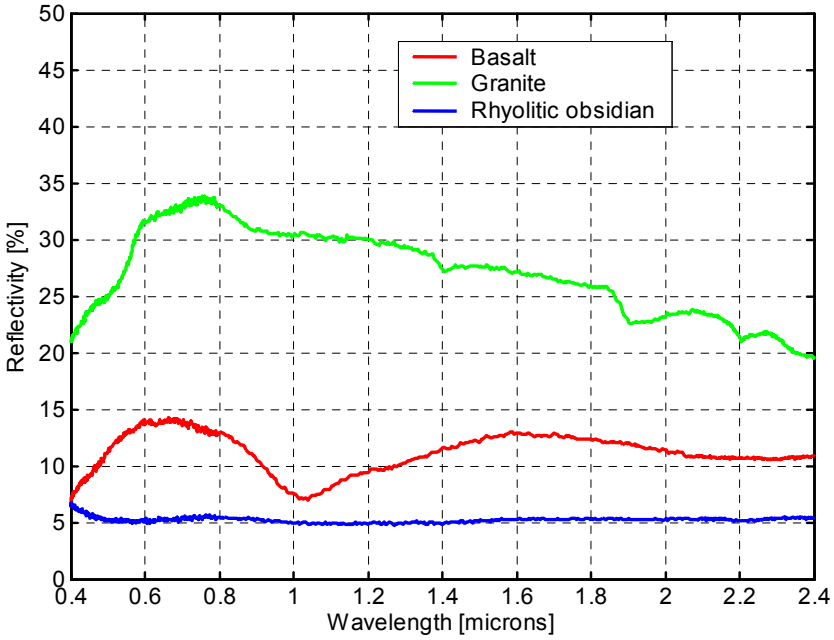

Figure 8. Laboratory reflectance spectra for three igneous rock examples.

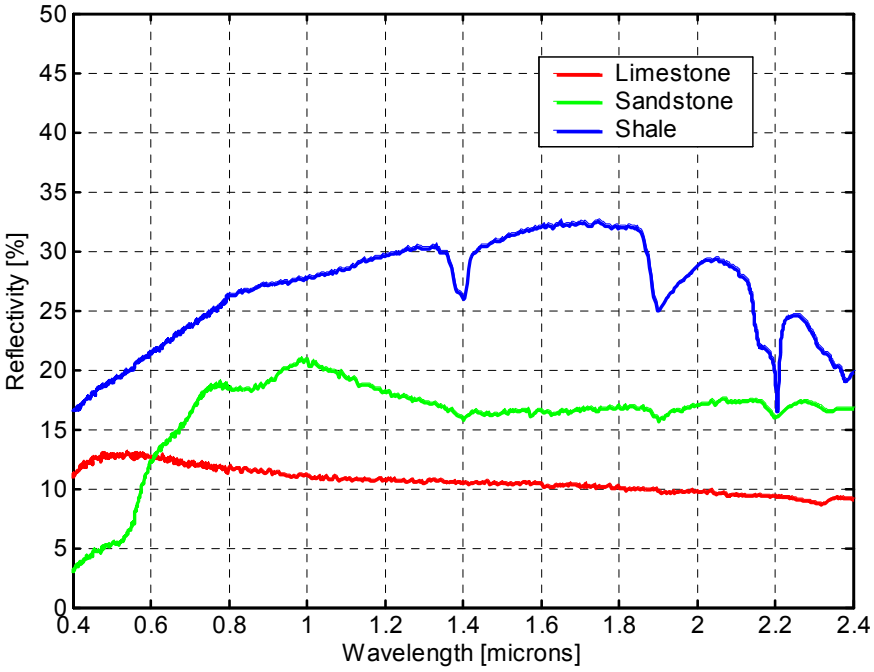

Figure 9. Laboratory reflectance spectra for three sedimentary rock examples.

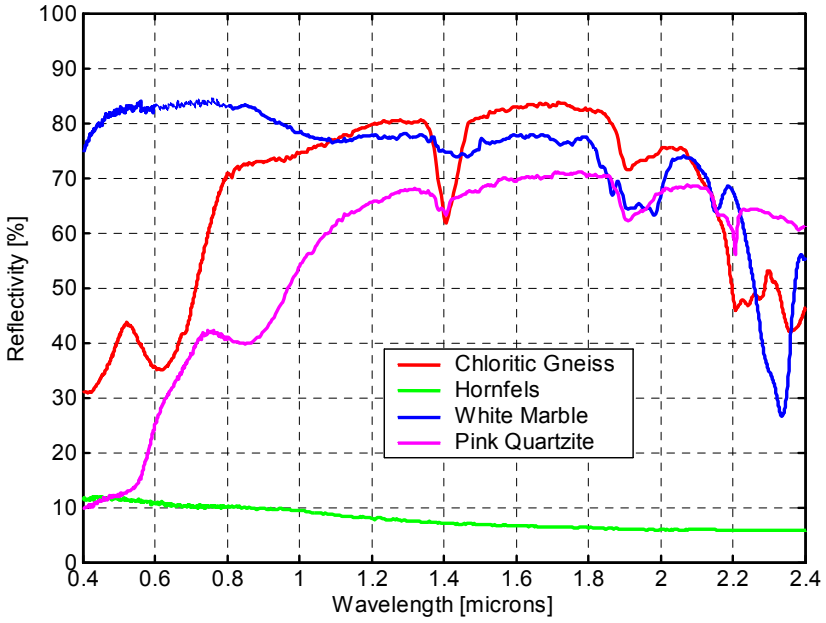

Figure 10. Laboratory reflectance spectra for four metamorphic rock examples.

Man-made Materials

The man-made materials class can be a very large one. For this application, we restrict out attention to man-made materials that would be commonplace in the remote sensing of a rural environment. Examples would include paving materials such as concrete and asphalt, and construction materials such as concrete, tar, pinewood, brick, cinders, and metals such as copper and galvanized steel.

Example laboratory reflectance spectra for road paving materials are shown in Figure 11. The reflectance spectra for these materials exhibit a generally slower rise in reflectivity from shorter to longer wavelengths, compared to the spectra for vegetation, soils, and some commonplace rocks. The maximum reflectivity is generally lower as well. The difference in reflectivity between wavelengths in the blue and red visible regions has been utilized to discriminate between paved road surfaces and shoulder materials for autonomous vehicle navigation [15]. Paved roads tend to be more bluish whereas materials encountered in road shoulders tend to be more reddish.

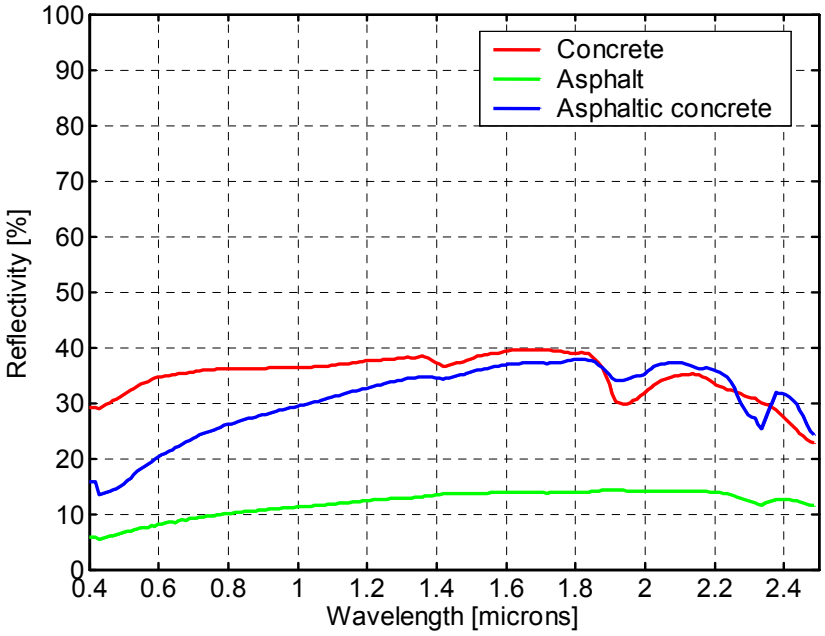

Figure 11. Laboratory reflectance spectra for road paving materials.

Example laboratory reflectance spectra for building materials are shown in Figure 12. Most of the construction materials in the figure are relatively featureless except for the general slow rise in reflectance starting at the shortest wavelengths. The construction pine wood is a notable exception, which exhibits the characteristics of senesced vegetation.

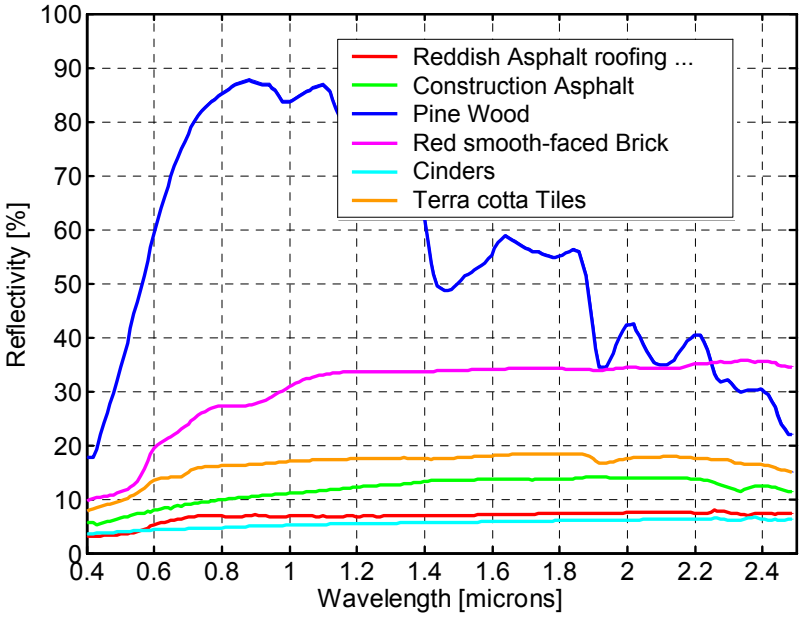

Figure 12. Reflectance spectra examples of building materials.

Water

A single example of the reflectance spectrum for seawater at Sea State 0 is shown in Figure 13. Although the absolute reflectivity can vary greatly depending on the viewing angle, the consistently negative slope in reflectivity from shorter to longer wavelengths appears to distinguish liquid water from many other materials.

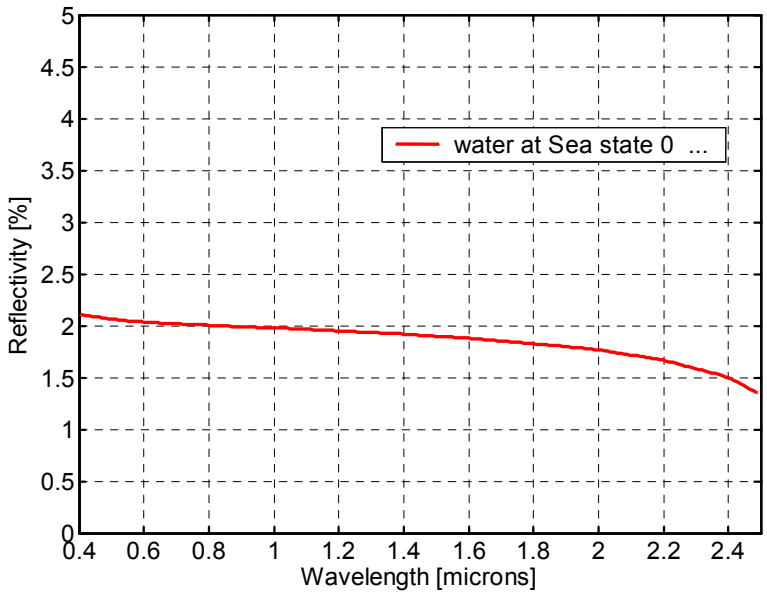

Figure 13. Reflectance spectrum for seawater at Sea State 0.

When water becomes frozen, it acquires the crystalline characteristics of a mineral. Consequently, the spectral analysis methods utilized for discriminating minerals also apply to the analysis of water ice.

Example reflectance spectra for frost and different granularities of snow are shown in Figure 14. The negative slope from shorter to longer wavelengths is still observable, particularly in the range of 0.6µm to 0.8µm. Narrow absorption features occur at 1.05µm and 1.21µm, and broad features occur at 1.30µm, 1.50µm, and 2.0µm.

Snow and frost can confuse the spectral analysis picture if the materials of interest are covered with it. Dealing with this issue is beyond the scope of this report.

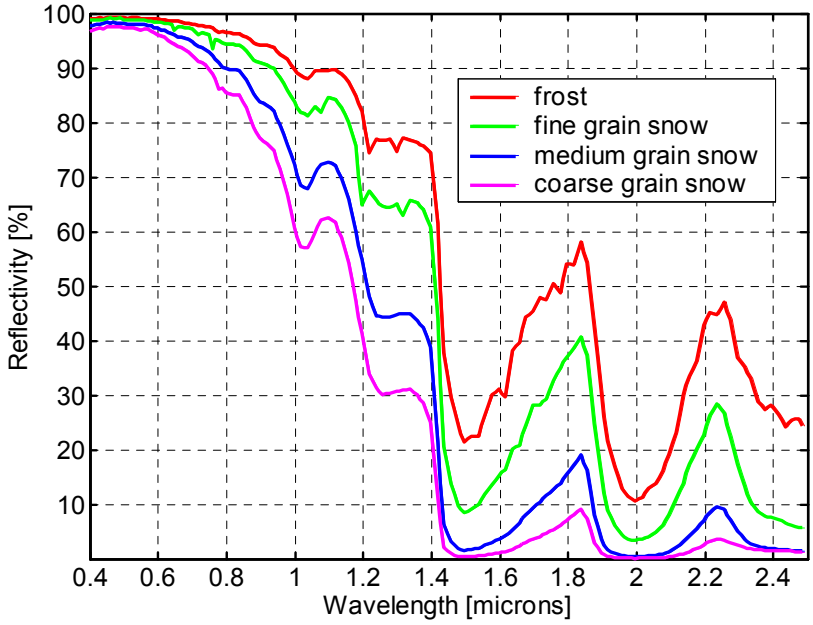

Figure 14. Reflectance spectra for water ice in the form of frost and snow.

Algorithm Strategies for Materials Identification

The primary emphasis of materials identification for autonomous navigation is on the discrimination of vegetation from other materials classes, and on the discrimination between vegetation species. The reason for this emphasis on vegetation is that the other materials classes consist of mostly very hard substances such as rocks and minerals, whose navigability is determined mostly by shape and position, independent of their chemical makeup. Conversely, the detailed shape of plants is determined by species.

Advantages of identifying plant species may include:

- Avoiding plant species that tend to snag small robotic vehicles
- Locating hidden water hazards by identifying plants that thrive at water's edge
- Seeking pathways below tree species that suppress undergrowth

Visible water hazards also deserve some attention since the detection of a body of water, or discriminating between dry soil and wet soil may have serious benefits with respect to navigability.

The ability of reflectance spectroscopy to discriminate between different materials is fundamentally limited by the number and fineness of the distinct wavelength bands one is able to measure. Consequently, it is appropriate to introduce the capabilities and complexities of multispectral and hyperspectral sensing, before delving into algorithm strategies.

Multispectral v. Hyperspectral Sensing

Multispectral sensors are commonly defined as those that measure in the neighborhood of 5 to 20 distinct wavelength bands. Hyperspectral sensors are commonly defined as those that are capable of measuring at least 100 distinct wavelength bands. Implicit with higher numbers of distinct wavelength bands is the need for sharper optical bandpass filters to separate the various bands. The spacing between adjacent measurement wavelengths can be 0.01μm, or perhaps finer, for hyperspectral sensors. Multispectral sensors typically have broader wavelength bands. A multispectral sensor example is provided in Table 5, which lists the sensing bands for the Landsat 7 Enhanced Thematic Mapper Plus (ETM+) [16].

Table 5. Landsat 7 ETM+ sensing bands.

Band Number	Wavelength Range	Description
1	0.45 – 0.515 μm	Blue
2	0.525 – 0.605 μm	Green
3	0.63 – 0.69 μm	Red
4	0.75 – 0.90 μm	Near Infrared
5	1.55 – 1.75 μm	Near Short Wave Infrared
6	10.4 – 12.5 μm	Thermal
7	2.09 – 2.35 μm	Middle Short Wave
Pan	0.53 – 0.90 μm	Color-InfraRed (CIR)

A digital RGB color camera could arguably be considered a minimalist multispectral sensor. However, for distinguishing vegetation from other material classes, substantial improvement would be gained by adding a single band centered at the vegetation plateau wavelength of 0.83μm, similar to Landsat 7 ETM+ band 4. Such technology exists today in a class of devices called Color-Infrared (CIR) sensors.

CIR sensors typically include at least two of the visible Red, Green and Blue wavelengths, plus at least one wavelength in the infrared. They exist as both still image cameras and video cameras. A still camera based on a Nikon N90 camera and modified by Kodak to obtain digital CIR capability was developed for the USDA Forest Service Remote Sensing Applications Center (RSAC). This digital still camera, shown in Figure 15, mimics the response characteristics of Panchromatic Color-Infrared (CIR) film utilized in remote sensing applications.

Figure 15. A still camera based on a Nikon N90, modified by Kodak for the USDA Forest Service, has digital Color InfraRed (CIR) capability.

A still picture of trees, grass, and sky, taken with the Kodak-modified CIR camera, is shown in Figure 16. The photo has been normalized to account for a fixed difference in sensitivity between the NIR and visible bands in the CIR camera. Reddish tints in the CIR image are indicative of photosynthetic vegetation.

Figure 16. Still picture of trees, grass, and sky taken with Kodak-modified CIR digital camera.

CIR video camera technology is also available. A video camera from the manufacturer *DuncanTech* that uses three CCD chips to obtain CIR capability is shown in Figure 17. The DuncanTech model is available in two standard configurations -- Green+Red+IR at full resolution, or Blue+Green+Red+IR at half resolution. Standard wavelength bands are listed in Table 6. DuncanTech camera technology is now sold through Kodak.

Table 6. Standard wavelength bands for the DuncanTech MS2100 CIR camera.

Color	Center Wavelength	FWHM
Blue	460 nm	45 nm
Green	540 nm	40 nm
Red	660 nm	40 nm
Infrared	800 nm	65 nm

Figure 17. DuncanTech model MS2100 CIR camera.

These CIR sensors are a bit cumbersome compared to what exists today in RGB still and video camera technology. However, the desired infrared band is within the spectral response of silicon CCDs, so there is no technical reason why a CIR camera can't be designed and built with the same sensor resolution and small packaging size of a modern color camera.

Another alternative is to utilize an RGB camera in conjunction with a laser radar operating at a wavelength of 0.83µm. The reflectivity image of the laser radar would provide data in the NIR to compare with the output of the RGB camera. Some calibration and image registration issues would need to be addressed, but it seems possible.

Jody Smith has suggested the following idea [2]. Two CIR cameras can be operated as a stereo pair. In order to register the frames from the two cameras, they need only have one wavelength in common. Thus, one camera can be R+G+B and the second camera can be R+G+IR, or even G+IR1+IR2.

A step up in complexity from CIR sensors is multispectral sensors that have up to perhaps 20 bands. These bands may span wavelengths ranging from 0.4µm to 2.5µm, which includes the VIS, NIR, and SWIR bands.

Typical silicon CCD arrays exhibit maximum responsivity at about 0.68µm with usable responsivity from 0.48µm to 0.96µm. Thus, to extend operation into the SWIR regime, sensing materials other than silicon are required. Indium-Lead (InSb) sensors can operate from approximately 1µm to 2.5µm. Indium-Gallium-Arsenide (InGaAs) sensors can operate from approximately 0.85µm to 1.7µm. Clearly, multiple sensing devices are required to span the VIS through SWIR wavelengths, and the multispectral sensor operating bands must be divided among these sensing devices.

The simplest mechanism for interposing the bandpass filters required to cover each band assigned to a particular device, is to place a spinning filter wheel in front of a staring 2-D sensor. The spinning filter wheel must be synchronized with image capture so that all pixels see the same filter during each image frame acquisition, and the sensor knows which filter is associated with each image frame.

Hyperspectral sensors are another step up in complexity from multispectral sensors in that they generate high-resolution data in three dimensions. Since most sensing elements are at most two-dimensional, some sort of mechanical scanning is required to obtain a third dimension. In a typical design, special optics are utilized to disperse received light at different wavelengths across one dimension of the sensor. The second dimension of the sensor yields one of the two required spatial dimensions, and the last spatial dimension is obtained by mechanically sweeping the sensor.

There are three possible types of optics used as filters to disperse light at different wavelengths across the sensing elements – prisms, transmissive holographic diffraction gratings, and reflective holographic diffraction gratings. Prisms are the simplest in design and exhibit the least amount of light attenuation. However, they produce nonlinear dispersion and have no aberration correction. Holographic diffraction gratings have linear dispersion and can be designed for aberration correction. However, they are more lossy than prisms. Transmissive diffraction gratings exhibit the highest losses allowing only about 5% of incident light to pass. Reflective diffraction gratings reflect 40 to 60% of incident light. Thus, reflective holographic diffraction gratings are the most popular optical design for modern hyperspectral sensors.

An important conclusion to draw from this discussion is that system complexity increases as the number of required wavelength bands increases, and the required wavelengths extend beyond the NIR band into longer wavelength bands. The relevant attributes are summarized in Table 7. The wavelength ranges stated in the table are approximate and are limited in scope to those of bands interest for the intended application. The sensor mechanics and detector materials are simply representative solutions – alternatives may exist.

Table 7. System complexity as a function of the desired number of wavelength bands and the range over which the desired wavelengths span.

Typical # of Bands	Wavelength Range	Sensor Type	Sensor Mechanics	Detector Material	System Complexity
3-4	0.4 – 1.0 μm	CIR	Staring 2D	Si	Low
5-7	0.4 – 1.0 μm	Multispectral	Filter wheel	Si	Medium
8-20	0.4 – 2.5 μm	Multispectral	Filter wheels	Si, InSb	Medium-high
>=100	0.4 – 2.5 μm	Hyperspectral	Scanning 3D	Si, InSb	High

Multispectral Algorithm Approaches

Spectral Features in the VIS/NIR

Much attention in the remote sensing of green vegetation is focused on the strong contrast in reflectance between the visible and NIR. A rapid transition, seen in Figure 4, occurs at a wavelength of approximately 0.7μm for healthy vegetation, and is often referred to as the *red edge*. The presence of the red edge is usually detected by comparing the reflectance at a wavelength below the red edge in the visible red region at about 0.68μm, with the reflectance at a wavelength above the red edge in the NIR region at about 0.83μm. Recall from earlier discussion that soil, which lacks the chlorophyll absorption feature at 0.68μm, and the strong reflectivity plateau at 0.83μm, exhibits weak red edge contrast that seldom exceeds that of even nonphotosynthetic vegetation.

If a particular remotely sensed scene contains a mixture of vegetation and exposed soil, the image pixels will exhibit varying degrees of red edge contrast depending on the relative proportions of vegetation to soil in each pixel. As a consequence, if a two-dimensional plot showing the distribution of reflectance values at the red vs. infrared wavelengths is formed, the result is a point cloud with a distinct appearance referred to as a tassled cap (Kauth and Thomas, 1976). Since the contrast between the two wavelengths for soil is usually less than or equal to the contrast for vegetation, soil establishes a baseline forming the flat bottom of the tassled cap, referred to as the "soil line". Conversely, vegetation tends to produce values in the point cloud that are approximately perpendicular to and above the soil line. Points that are most distant from the soil line represent pixels that contain 100% vegetation. This discovery led to a number of algorithm strategies for detecting the soil line, and establishing various indices for detecting vegetation above the soil line.

The ratio vegetation index was developed as an approximate measure of the proportion of vegetation in each pixel (Jordan, 1969), which has the form

$$RVI = \frac{\rho_{NIR}}{\rho_{RED}} \quad , \qquad \text{(Eq. 1)}$$

where ρ is reflectance.

Unfortunately, *RVI* has an infinite range of values. The normalized difference vegetation index (*NDVI*) is functionally related to RVI, but has the advantage of being bounded to the range of -1.0 to 1.0. It has another advantage in that it tends to reduce the effects of broadband albedo through normalization.

$$NDVI = \frac{\rho_{NIR} - \rho_{red}}{\rho_{NIR} + \rho_{red}} = \frac{RVI - 1}{RVI + 1} \qquad \text{(Eq. 2)}$$

The *NDVI* was computed for every laboratory reflectance spectrum in the merged database. The NDVI wavelengths were 0.68μm and 0.83μm. The results were grouped into histograms for each broad material class, which are shown in Figure 18. The five-character class tags for each material category are shown above the histograms.

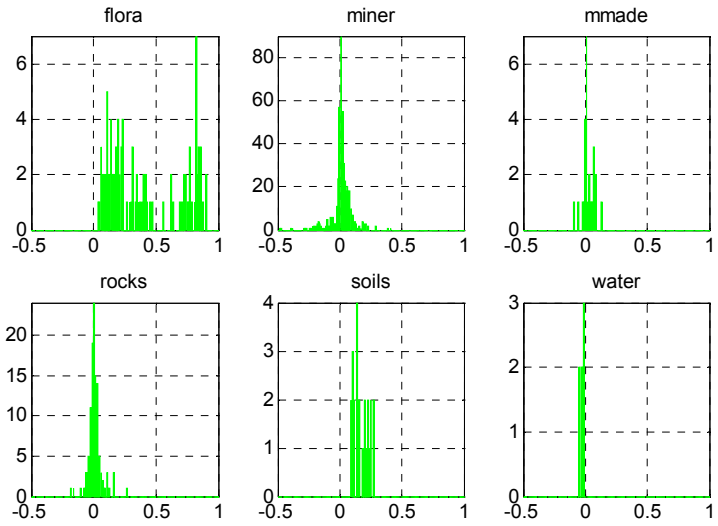

Figure 18. Histograms of NDVI values computed from reflectance spectra in the merged database.

Note that the NDVI is positive for each vegetation instance in the database. It also has a bimodal appearance with a split at a NDVI value of about 0.5. This bimodal character may be due to clustering of photosynthetic and nonphotosynthetic vegetation. The largest NDVI value for non-vegetation (~0.42) occurred in the mineral class. Thus, a NDVI value greater than 0.42 separates a substantial amount of photosynthetic vegetation from all other classes.

Soils exhibited positive-only NDVI values in the range of 0.09 to 0.27. Water exhibited NDVI values that were all negative. Thus, NDVI appears to easily separate vegetation from water in laboratory spectra. The other material classes – minerals, rocks, and man-made materials – exhibited NDVI values that were both positive and negative. Thus, NDVI has some ability to reject a portion of these material classes, but additional discriminants are needed to fully separate these classes from the vegetation class.

The normalized difference operator has inspired researchers to seek other pairwise combinations of wavelengths that might exhibit some discrimination power with respect to vegetation health. A small sampling of these operators is listed in Table 8.

Table 8. A small sampling of other normalized difference and related operators.

Operator	Description	Wavelengths (μm)
PNI	Percent Nitrogen	0.764, 1.640
PRI	Photochemical Reflectance	0.531, 0.570
PNSI	Plant Nitrogen Spectral Index	$PNSI = \text{abs}(1/NDVI)$
RVSI	Red Edge Vegetation Spectral Concavity	$(\rho_{0.714} + \rho_{0.752})/2 - \rho_{0.733}$
NDGR	Normalized Difference Green-Red	0.670, 0.550

Many of the operators listed in Table 8 are designed to measure some aspect of plant health. The normalized difference green-red (NDGR) operator tends to measure the "greenness" of materials, and is of more general use.

Histograms of the NDGR operator computed for each material class in the merged database are shown in Figure 19. Note that approximately half of the flora class has NDGR values less than zero and the other half has values greater than zero. Vegetation that has color more green than red, has positive NDGR values. Soil colors are more red than green. All the soil instances in the merged database have NDGR values that are less than zero. Relatively high percentages of minerals, rocks, and man-made materials also have NDGR values that are less than zero.

Things get more interesting when one combines the NDGR results with the NDVI results. Vegetation that is photosynthetic and not senesced, have strong positive NDVI values. Among the vegetation that falls within this category, the NDGR index tends to discriminate between branches and leaves. Thus, negative NDGR values tend to identify tree bark and branches, and positive NDGR values tend to identify leaves.

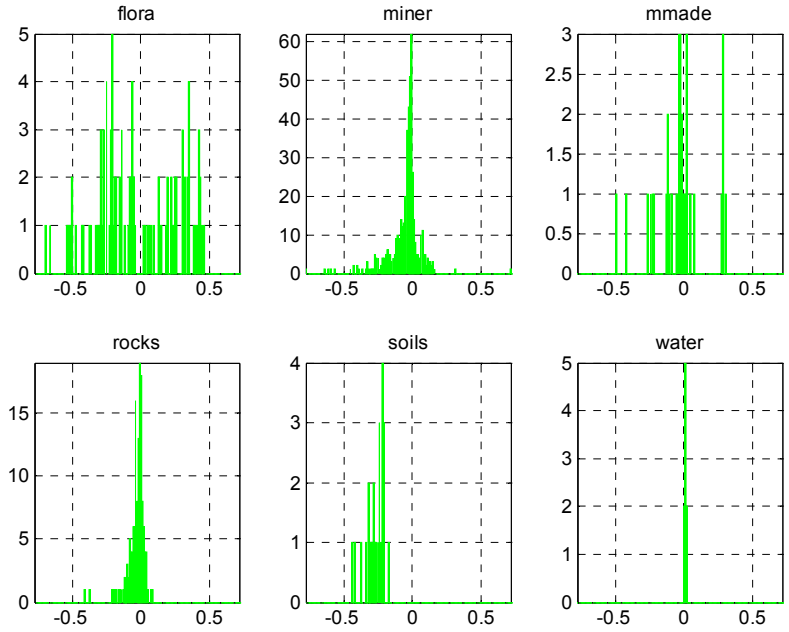

Figure 19. Histograms of NDGR values for broad material classes.

A comparison of wavelengths in the visible red region with wavelengths in the visible blue region has been utilized in autonomous navigation for road following to discriminate between road paving materials and materials encountered on the road shoulder [15]. A normalized difference discriminant can be formed based on these two wavelength regions. Here we define a normalized difference blue-red (NDBR) operator as

$$NDBR = \frac{\rho_{blue} - \rho_{red}}{\rho_{blue} + \rho_{red}} \quad . \qquad \text{(Eq. 3)}$$

Using a center wavelength of 0.48μm in the visible blue region, and a center wavelength of 0.67μm in the visible red region, histograms of the NDBR were computed for the material classes. The results are shown in Figure 20.

Note that all soils in the database have NDBR values that are less than -0.25. Of the man-made materials in the database, all road paving materials have NDBR values greater than –0.25. This reinforces the claims that blue-red differences can discriminate between paved road materials and roadside dirt.

Some man-made materials that had NDBR values less than –0.25 were pinewood, red brick, and roofing shingles.

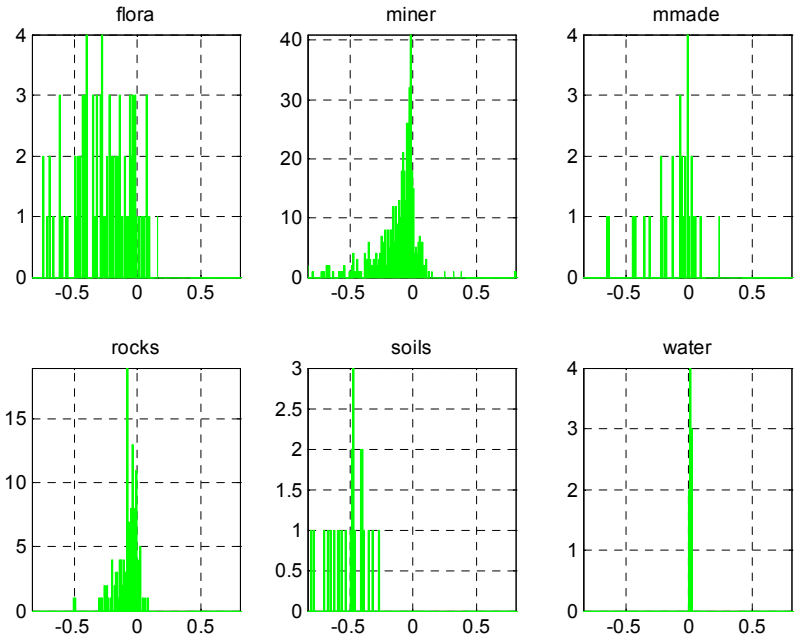

Figure 20. Histograms of the NDBR discriminant for the broad material classes.

The NDVI, NDGR, and NDBR discriminants can be computed using either broad or narrow wavelength regions. They need only have the proper center wavelengths with minimal overlap. This means that they can be obtained from CIR, multispectral, or hyperspectral systems.

A stereoscopic CIR approach that utilizes the NDVI, NDGR and NDBR discriminants is appealing due to low system complexity. If the CIR camera pair has at least one

wavelength in common, the images can be co-registered, and range information can be derived from binocular disparity. Range information is essential for deducing object scale. If combined with broad spectral information, objects can be segmented within a scene.

If one adds texture analysis to augment materials identification, it may be possible with a completely passive system to meet the autonomous navigation object avoidance goals in daylight.

An interesting alternative would be to combine a single RGB camera with laser radar operating at a wavelength of 0.83μm. The possibility of combining NIR reflectance data from the laser with the RGB wavelength data from the camera to obtain the equivalent of CIR capability deserves further investigation.

Spectral Features beyond VIS/NIR

Spectral features beyond the visible and NIR bands include the vegetation absorption features due to cellulose, lignin, and nitrogen, the soil absorption feature due to clay minerals, and the absorption features of rocks and minerals due to their crystalline structure and molecular constituents. In this section we will explore how to utilize limited numbers of these features to discriminate between broad material classes. However, the narrowness of some features requires that the filters for the wavelength features be highly selective. Thus, the total number of features implies multispectral sensing, but the sharpness of the filters implies hyperspectral wavelength resolution. Perhaps, we can call our hybrid approach *finespectral* sensing.

Toward that end, the merged database of laboratory reflectance spectra was re-sampled to a uniform wavelength spacing of 0.01μm. Our analysis is confined to the wavelength range of 0.4μm to 2.4μm.

Faced with a bewildering array of absorption features exhibited in the various material classes, we sought to employ a feature discovery mechanism for determining the best features for separating the material classes. The approach consists of the following steps: 1) forming a normalized difference index (NDI) for every possible pairwise combination of wavelengths at 0.01μm intervals, 2) computing receiver operating characteristic (ROC) curves from the normalized difference indices, for separating one material class from every other material class, and 3) forming a performance metric by computing the maximum area under each ROC curve.

The ROC curves were formed by computing the probability of detection and the false alarm rate for each normalized difference metric, at 100 equally-spaced detection threshold values, spanning the full range [-1 1] of possible normalized difference values. The area under the ROC curves was computed for each pairwise combination of wavelengths. Those combinations of wavelengths that yielded the greatest area under the

ROC curve were deemed to have the greatest discrimination power for separating the material classes.

The result for separating the vegetation class from all other material classes is shown in Figure 21. Each colored pixel in the figure represents the area under the ROC curve for a normalized difference index computed from two specific wavelengths. The black diagonal line that runs through the figure indicates the ROC areas obtained from normalized difference indices computed for the cases where the two feature wavelengths were equal. Clearly, when the wavelengths are equal, the discrimination power is zero.

The dark red regions in the figure indicate pairwise combinations of feature wavelengths that exhibit strong discrimination power. Note that the NDVI discriminant has been re-discovered by the process, as indicated by the dark red region centered at about 0.6μm in the first feature wavelength, and spans approximately 0.7μm to 1.1μm for the second feature wavelength. A contour plot of the same data would reveal more precise information.

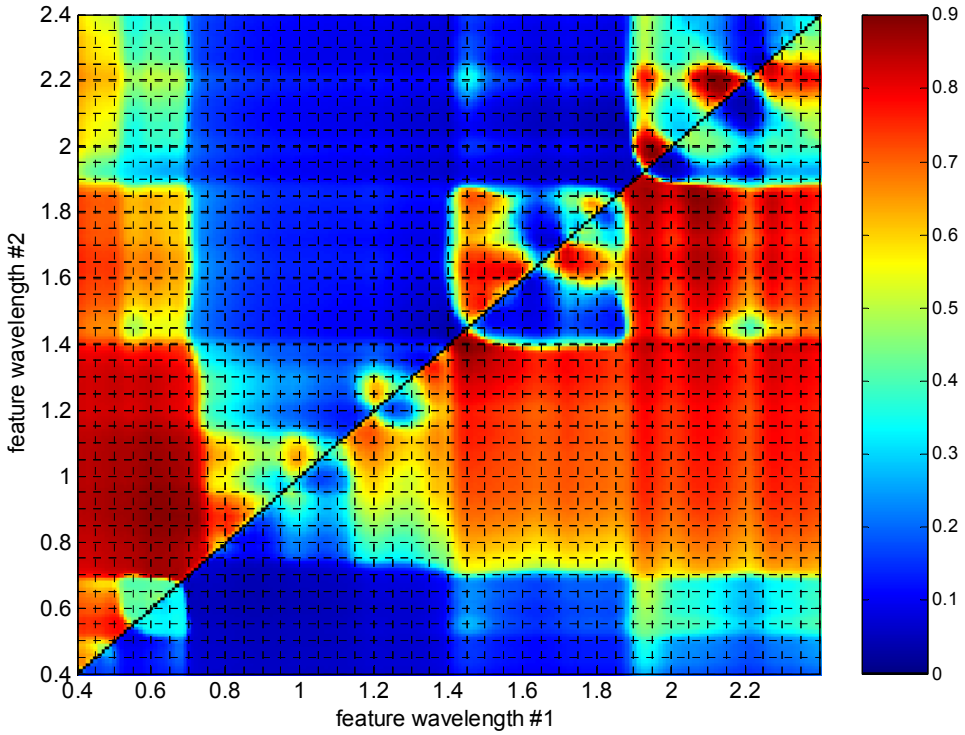

Figure 21. Color-coded plot of ROC curve areas for every pairwise combination of feature wavelengths from which normalize difference indices were computed. Dark red regions represent wavelength combinations with the greatest discrimination power.

The result in Figure 21 does not take into account the effects of atmospheric absorption. Recall from earlier discussion that reflectance in certain wavelength bands is highly variable, and in some cases, practically immeasurable, due to atmospheric absorption. The same plot is repeated in Figure 22, with these problematic wavelength bands blocked

out. The dark red regions in this figure represent candidate feature wavelength pairs for discriminating vegetation from the other material classes.

Thirteen pairs of wavelength features were extracted at local maxima found in the red regions in the figure. These wavelength pairs are listed in Table 9. An attempt was made to associate the extracted wavelengths with known feature wavelengths in the published literature. Most feature wavelengths listed in the table have associations with known absorption feature wavelengths and/or known high reflectance regions for vegetation, i.e. the vegetation plateaus.

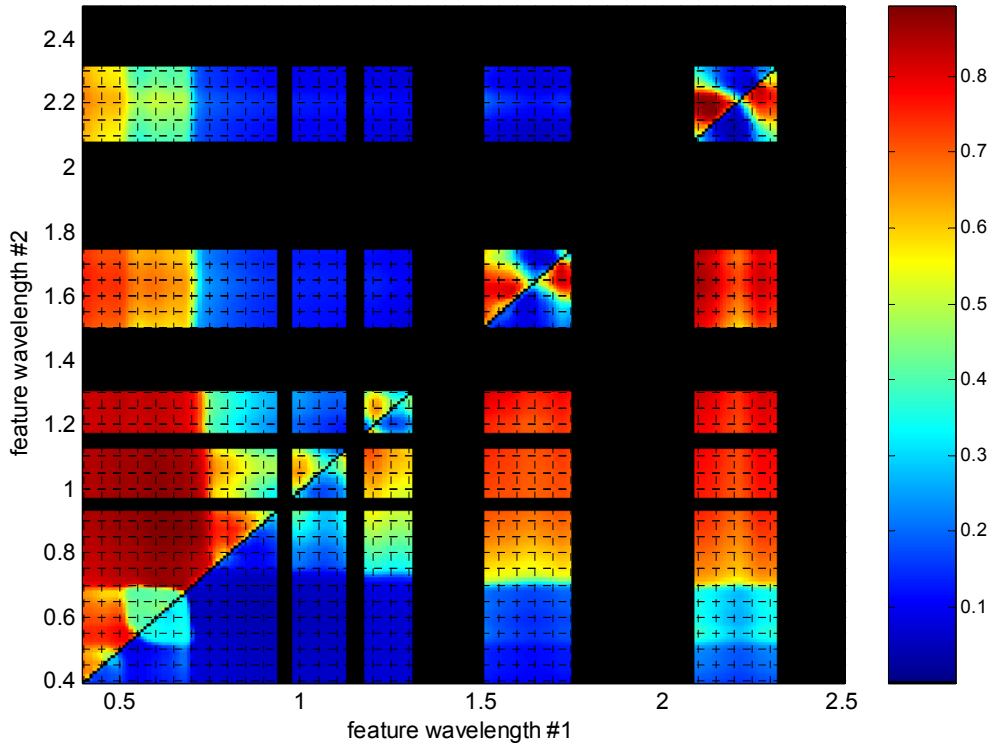

Figure 22. ROC curve areas with atmospheric absorption wavelength regions blocked out.

The thirteen feature wavelength pairs were tested using a uniformly weighted linear classifier, in which every possible subset of these features was considered. The purpose was to retain only the most discriminating features, and to reject those features that did not significantly contribute to overall performance. The same area under ROC curve metric was used for the evaluation.

The surviving feature pairs were #1, #2, #4, #5, #7 and #12. A final experiment was then conducted in which randomly valued weights were applied to each feature pair in a large Monte Carlo run. The weights were chosen randomly, but were scaled to sum to unity.

The weights that maximized the ROC curve area, drawn from one million random combinations, are listed in Table 10.

Table 9. List of wavelength feature pairs extracted from local maxima in the red regions of the ROC area plots.

Pair Number	Feature λ #1	Wavelength #1 Associations	Feature λ #2	Wavelength #2 Associations
1	0.64	Chlorophyll	0.89	Vegetation plateau
2	2.12	Lignin	2.19	Vegetation plateau
3	2.10	Arabinogalactan, Cellulose, Lignin, Starch	1.65	Vegetation plateau
4	2.27	Lignin, Cellulose	2.24	Pectin (apple)
5	1.72	Pectin (apple), Xylan	1.68	D-ribulose, Lignin, Pectin (citrus)
6	2.27	Lignin, Cellulose	1.65	Vegetation plateau
7	1.57	unknown	1.62	Vegetation plateau
8	0.51	Humic acid	0.54	Humic acid
9	0.40	Chlorophyll-a, Humic Acid, Lutein	1.65	Vegetation plateau
10	0.40	(same as above)	0.44	a-carotene, Chlorophyll-a, Chlorophyll-b, Humic Acid, Lutein, Protochlorophyll
11	0.40	(same as above)	2.21	Vegetation plateau
12	1.21	Arabinogalactan, Carnauba wax, Xylan	1.25	Vegetation plateau
13	1.00	unknown	1.05	Vegetation plateau

Table 10. Surviving feature pairs and relative weighting in a linear classifier.

Pair #	Wavelength #1	Wavelength #2	Weight Value
1	0.64	0.89	0.0695
2	2.12	2.19	0.2445
4	2.27	2.24	0.0868
5	1.72	1.68	0.2900
7	1.57	1.62	0.2545
12	1.21	1.25	0.0547

The ROC curve shown in Figure 23 indicates the ability of the weighted combination of six normalized difference index features to separate the vegetation class from all other material classes in the database. With the threshold set for a probability of detection of 100% for vegetation, the system rejects 47 out of 50 instances of the other material

classes. It should be noted that this is the performance that would be obtained for a one-pixel observation of the data. Better performance would be expected for multiple pixels.

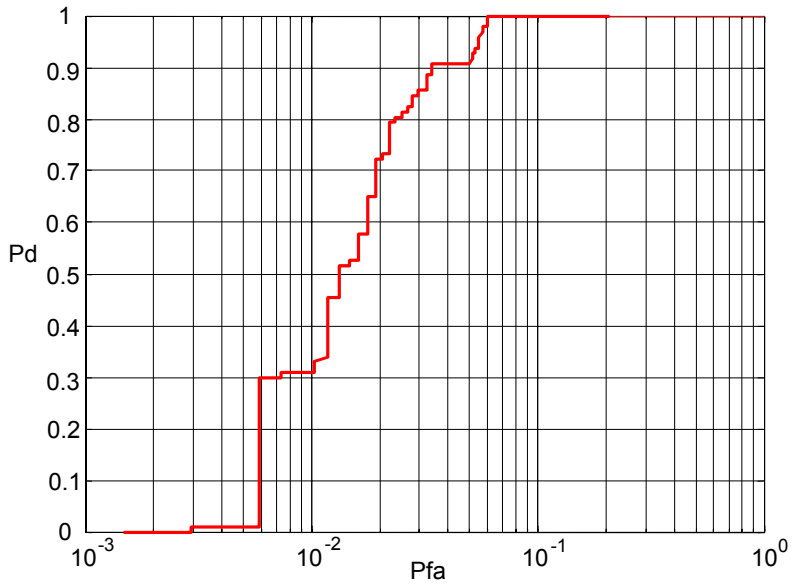

Figure 23. Single pixel observation ROC performance curve for discriminating vegetation from all other material classes.

Atmospheric Corrections

The normalized difference indices (NDI) utilized in the previous section provide some measure of compensation for variation in the reflectance spectra of materials due to atmospheric effects. This is because they are based on reflectance ratios rather than absolute measurements. However, additional compensation for atmospheric effects may be required.

A calibration of atmospheric conditions can be performed under laboratory conditions with an accuracy of perhaps 2.5%. A 5% error is the best that can be achieved in the field using high quality equipment, careful technique, and the best atmospheric modeling codes available. A calibration accuracy of 10% could be expected for a real-world deployable system [2].

In order to achieve 10% accuracy, the following two items are needed 1) characterization of atmospheric aerosols, and 2) characterization of columnar water vapor. Additional items could be measured, but these two items yield the biggest payoff.

Atmospheric aerosols can be characterized by local measurement of direct and diffuse light. Conceptually, a device would be mounted on top of the robotic vehicle that would measure the spectrum of direct sunlight, as well as diffuse light over a full hemisphere. Both measurements would be taken over a selected set of wavelengths.

The Yankee Environmental Systems Multi-Filter Rotating Shadow-Band Radiometer (MFRSR) is a commercial device designed to measure direct and diffuse radiation at six wavelengths: 0.415, 0.500, 0.610, 0.665, 0.862, and 0.940 μm. The nominal full width half max (FWHM) bandwidth is 0.01μm [17,18].

Columnar water vapor can be measured using two wavelengths – either 0.94μm and 0.87μm, or 0.94μm and 1.03μm. The 0.94μm wavelength is in the middle of an H_2O absorption feature, and 0.87μm and 1.03μm are on the edges on either side of the absorption feature. The columnar water vapor is characterized by computing a linear regression of the data at the middle and at either edge of the H_2O absorption feature.

A miniature instrument designed to characterize both aerosols and columnar water vapor could be designed for a small robotic vehicle. The maximum calibration error would be at the longer wavelengths. An instrument with a calibration error of 10% at 2.4μm would have as little as 2% calibration error at 0.5μm.

In the autonomous navigation application, the close proximity of the vehicle to the potential obstacles whose reflectance is being measured would ensure that the atmospheric compensation measured at the vehicle would be valid at the obstacle location.

Hyperspectral Algorithm Approaches

Continuum Removal

The remote sensing of surface materials from satellites in space is a more difficult challenge than sensing the same materials near the earth's surface, due to the additional return path through the atmosphere required to reach the sensor. As such, drastic measures are taken in satellite sensing to discount the effects of atmospheric variations in radiance measurements.

A process called *continuum removal* is often used, which involves constructing a piecewise linear convex hull, or polynomial continuum across the peaks of a reflectance spectrum, and dividing the reflectance value at each wavelength by its continuum value [19]. This compensates for curvatures and tilts in localized regions of the radiance spectrum due to atmospheric variations.

A more localized continuum removal is performed when one is interested in spectral detail in selected wavelength ranges. The sequence of steps for constructing a localized continuum is pictured in Figure 24 through Figure 27, for the reflectance spectrum of dry tumbleweed.

A continuum region is defined by the wavelength endpoints of a continuum line, and a predetermined central wavelength somewhere between the two endpoints. In the first algorithm step, the reflectance values at the endpoint wavelengths are obtained. In the second step, the reflectance values at each measured wavelength at and between the

endpoints are divided by the reflectance values along the continuum line. This step removes the tilt from the continuum region, as shown in Figure 25.

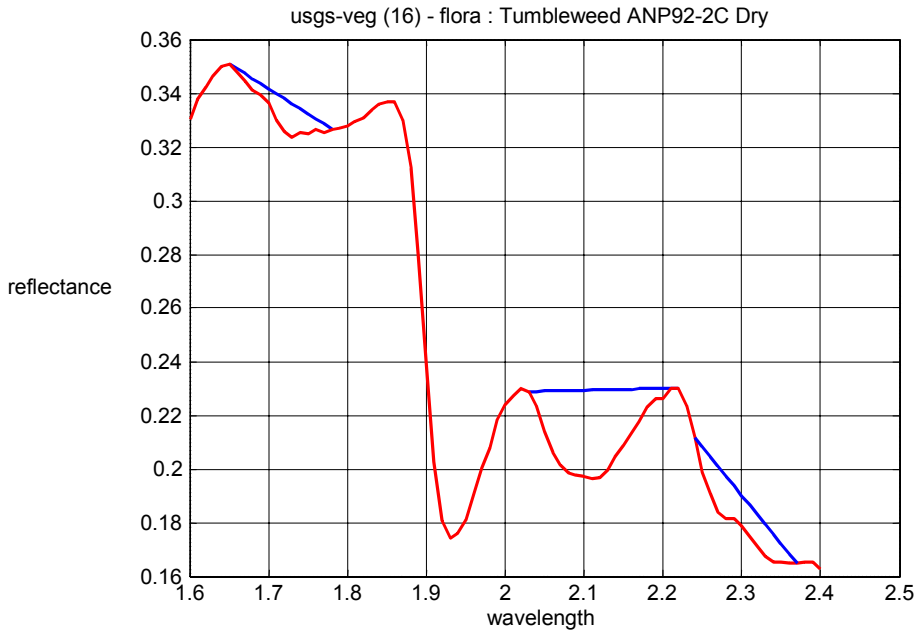

Figure 24. Continuum lines shown on the reflectance spectrum of a tumbleweed.

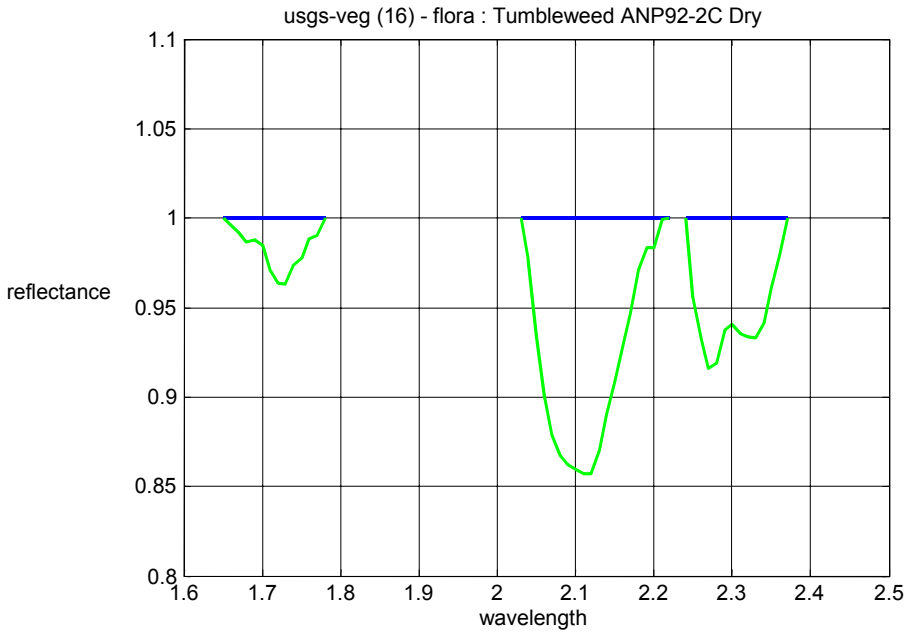

Figure 25. Local continuum have been extracted and the spectral values have been divided by values along the continuum line. The continuum lines have been vertically biased to a reflectance value of one.

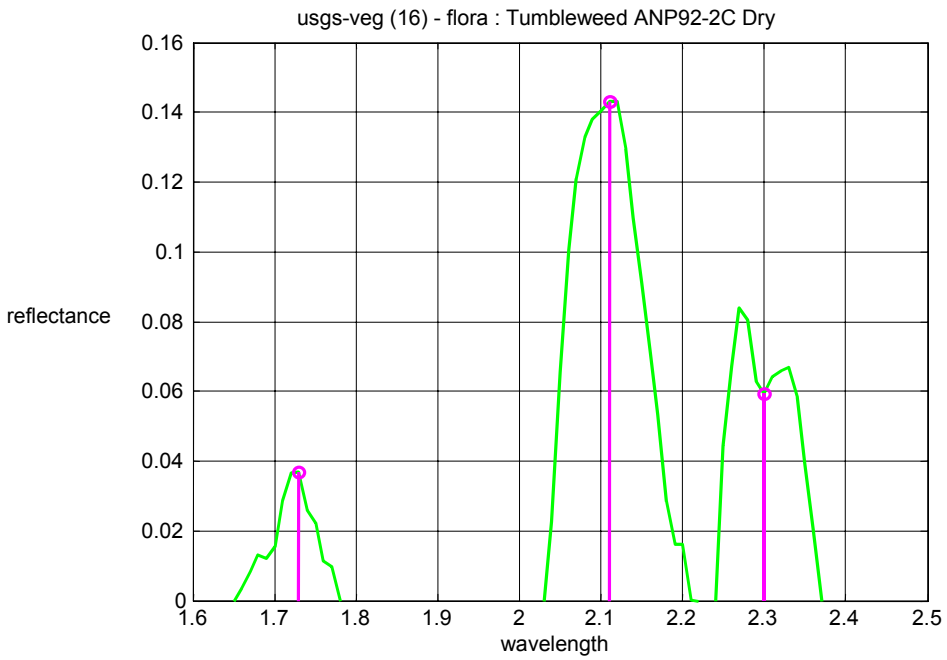

Figure 26. The reflectance values have been inverted, and the reflectance at the continuum center wavelengths have been measured.

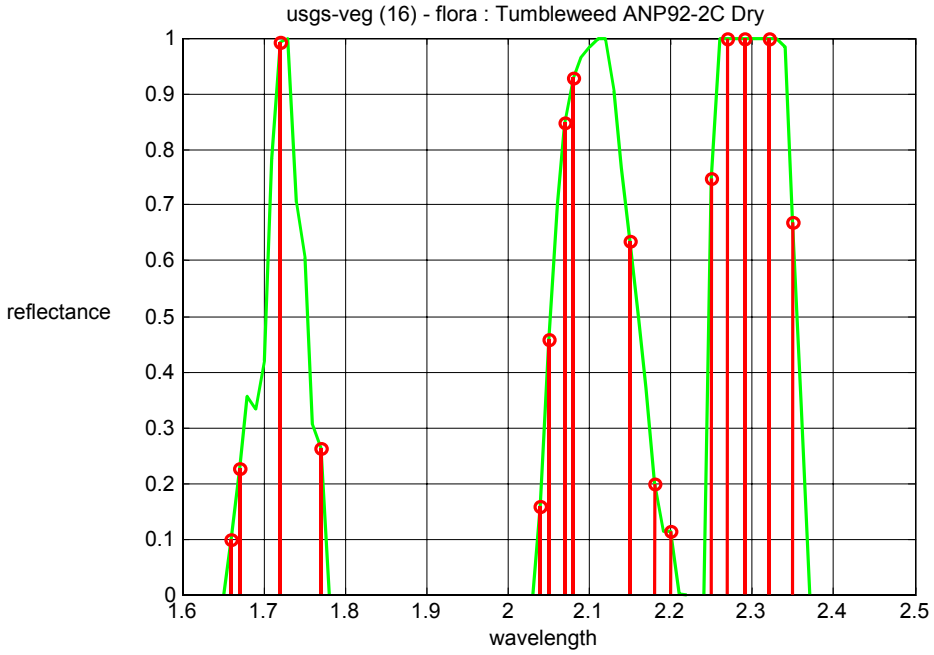

Figure 27. Reflectance values in the continuum regions have been normalized by the reflectance measured at the continuum center wavelengths. Measurements of normalized reflectance are then taken at predetermined wavelengths within each continuum region. These measurements are more stable under atmospheric variation.

In the third step, the reflectance values are inverted and the continuum lines are at zero reflectance, along the horizontal axis. The reflectance value at the central wavelength defined for each continuum, is also obtained. In the final step, the reflectance values are normalized by the central reflectance values obtained in the previous step. The new reflectance values now peak at 1.0.

With the reflectance samples in the continuum now compensated for atmospheric variation, and normalized in amplitude, measurements at critical wavelengths within the continuum can now be taken, and used in an absolute magnitude sense. The critical wavelengths within the local continuum are usually absorption wavelengths that tend to discriminate between different materials of interest.

One can go through the exercise of constructing local continuum regions optimized for the discrimination of vegetation. However, for the autonomous vehicle obstacle avoidance problem, given that the measurements are taken close to the earth's surface, and given the possibility of characterizing the atmosphere to 10% accuracy in close proximity to the materials being measured, it may not be necessary to perform continuum removal.

Materials Identification Using Hyperspectral Data

A basic starting point for pursuing materials identification with hyperspectral data is to utilize the measured reflectance obtained at each wavelength as a set of raw features. We seek to identify selected vegetation species while rejecting all other plants and materials. The hope is that the pattern of reflectance as a function of wavelength is distinct between different plant species compared to within-class variation.

A first check is to determine the separability of the exemplars available in the database for each plant species of interest. There are a number of distance measures used to determine separability [1]. One of the simplest distance measures is an angular metric defined as

$$ANG = \cos^{-1}\left(\frac{\mu_a^T \mu_b}{\|\mu_a\| \cdot \|\mu_b\|}\right) \qquad \text{(Eq. 4)}$$

Where μ_a is the feature vector for some material a, and μ_b is the feature vector for a second material b. Small angle values for the metric indicate low separability, and larger angles indicate higher separability.

Experiments have been performed with two plant species – tumbleweed and aspen leaf – representing dry nonphotosynthetic and green photosynthetic instances. Each of the two species was considered the target class in separate experiments. In both cases, the non-target class included all other plant species in the database, and where appropriate, all other material classes.

A laboratory reflectance spectrum for the tumbleweed is shown in Figure 28. The reflectance values at wavelengths with high atmospheric absorption are not displayed. These wavelengths have been eliminated from consideration as features.

The angular separability metric was computed for the tumbleweed instance measured against all other vegetation instances in the database. The result is shown in Figure 29. The database index number for each vegetation instance is represented on the horizontal axis. The tumbleweed is at index number 16, which shows the expected angular separation of zero. Most vegetation species were separated from the tumbleweed by at least 5 degrees. There were 8 out of 96 vegetation instances in the database that yielded angular separation of less than 5 degrees. The closest was brown wood from Big Sagebrush, with an angular separation of 2.2 degrees. Other instances included brown wood, bark, and leaves from Mormon Tea, White Peppermint, and Sycamore.

Next, the angular separability was computed for the tumbleweed measured against other material classes in the database including vegetation, soils, rocks, minerals, and man-made materials. The result is shown in Figure 30. The first 96 database entries are vegetation. Beyond these entries, separability from the other materials was, on average, noticeably greater. The closest non-vegetation match was a mineral called Saucenite at index #498, with a separability angle of 6.5 degrees.

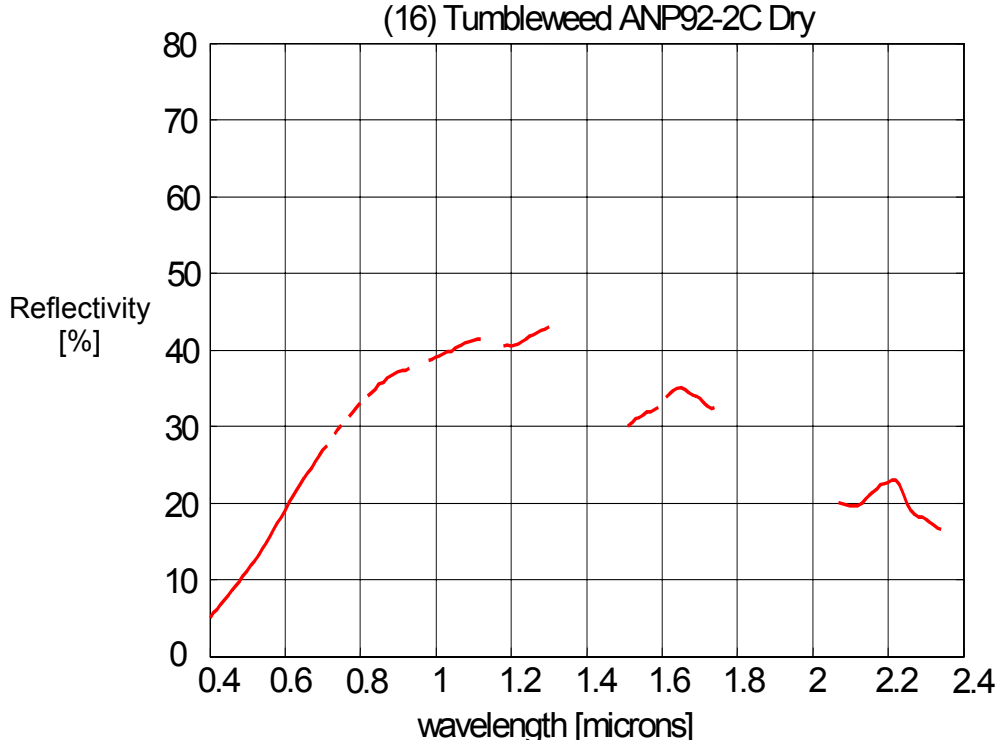

Figure 28. Laboratory reflectance spectrum of tumbleweed. Reflectance values at strong atmospheric absorption wavelengths are eliminated.

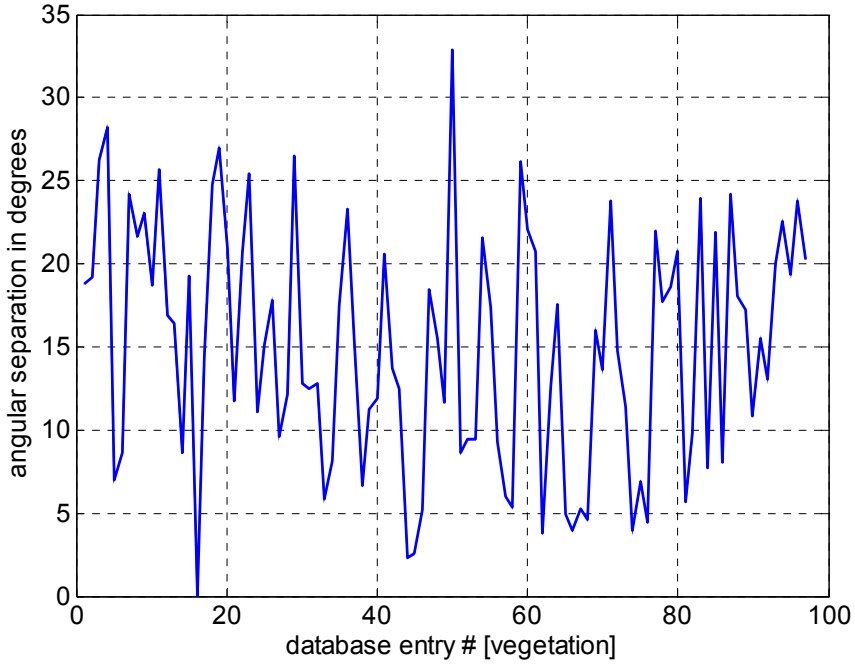

Figure 29. Angular separation in degrees between the tumbleweed instance and all other vegetation instances in the database. Database entry #16 is the tumbleweed itself, so the angular separation value is zero.

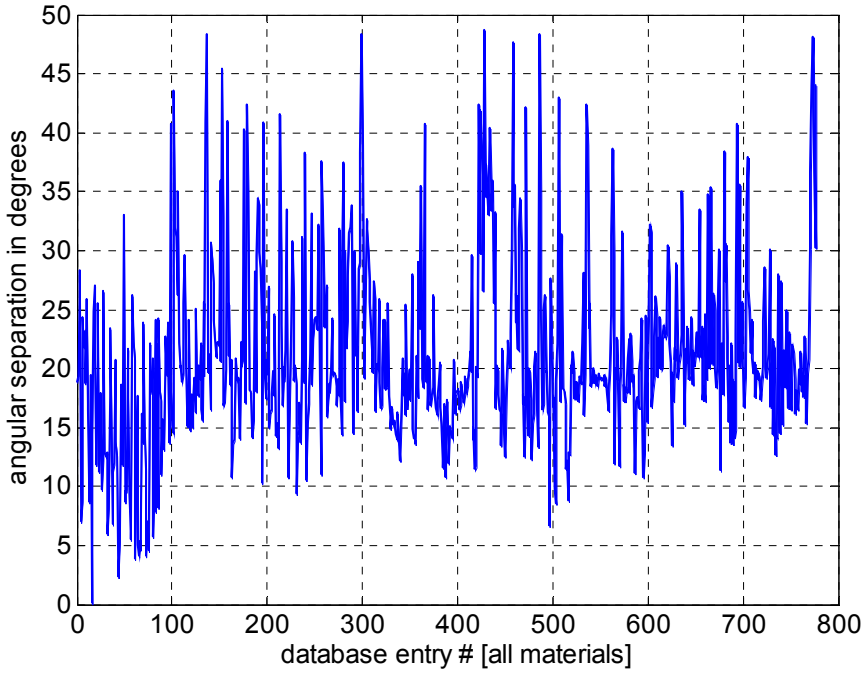

Figure 30. Angular separation in degrees between the tumbleweed instance and all other materials in the database.

Next, the experiments were repeated for the aspen leaf. The reflectance spectrum for an instance of the Aspen leaf is shown in Figure 31. The angular separability metric was computed for the Aspen leaf instance measured against all other vegetation instances in the database. The result is shown in Figure 32. There are actually two instances of the Aspen leaf in the database at indices #1 and #2. The within-class separation between these two instances is 0.79 degrees. There are 12 out of 94 instances of other vegetation that exhibit separability angles of less than 5 degrees. The closest is a Maple leaf at 2.4 degrees, followed by Red Willow and Bay Laurel.

The separability for materials in other classes is very strong. The median separability angle is 34.3 degrees. The mineral Sphalerite is the closest non-vegetation match at 17.5 degrees.

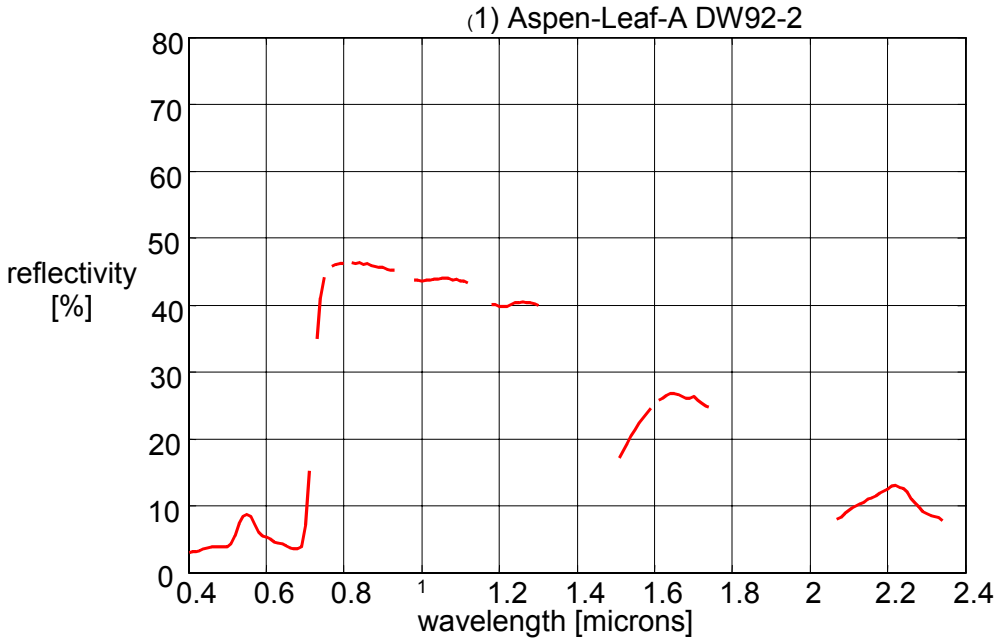

Figure 31. Laboratory reflectance spectrum of an Aspen leaf. Reflectance values in atmospheric absorption bands are not shown.

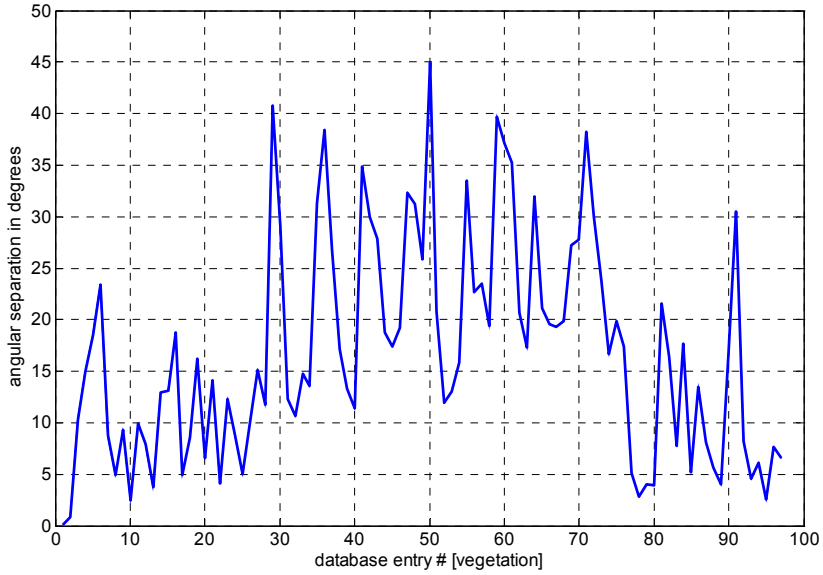

Figure 32. Angular separation in degrees for an Aspen leaf measured against other vegetation. Two instances of the Aspen leaf are at database indices #1 and #2.

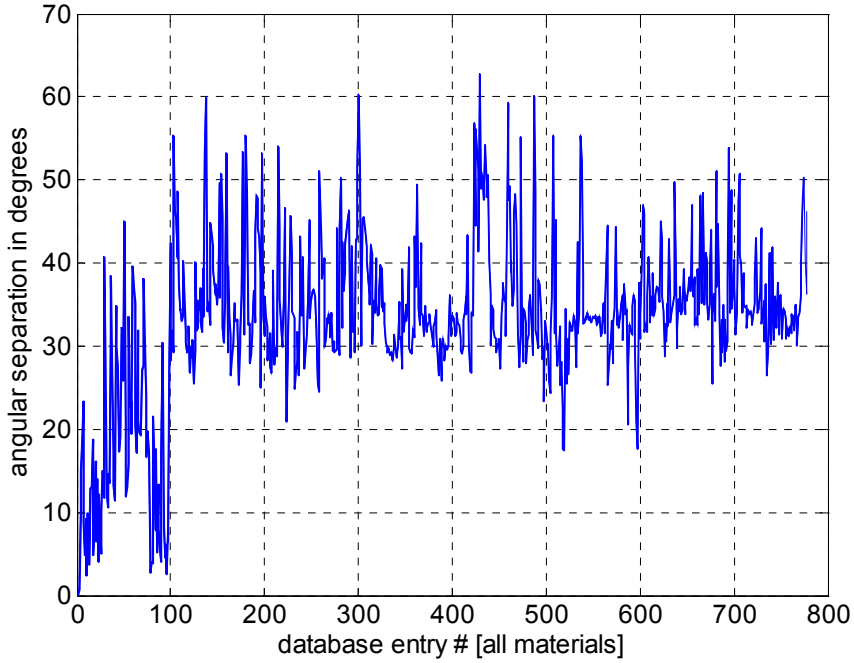

Figure 33. Angular separation in degrees between the Aspen leaf instance and all other materials in the database. The median separation for non-vegetation materials, which begin at index #96, is 34.3 degrees.

Since the database only contains one or two instances of individual plant species, it is difficult to assess within-class variation. One attempt at gaining some insight into this matter was made in the form of an experiment. One of the Aspen leaf reflectance spectra was mixed with the reflectance spectrum of a brown loam soil, in controlled proportions. The resulting angular separation between the original Aspen leaf spectrum and the mixed spectrum is plotted in Figure 34 as a function of the percentage contribution of the soil spectrum. The relationship between the percent soil mixture and the angular separability appears to be linear. A mixture of 5% soil and 95% Aspen leaf is enough to add 5 degrees of angular difference compared to the pure Aspen leaf exemplar. This amount of within-class separation could be enough to confuse the Aspen leaf with its closest match the Maple leaf.

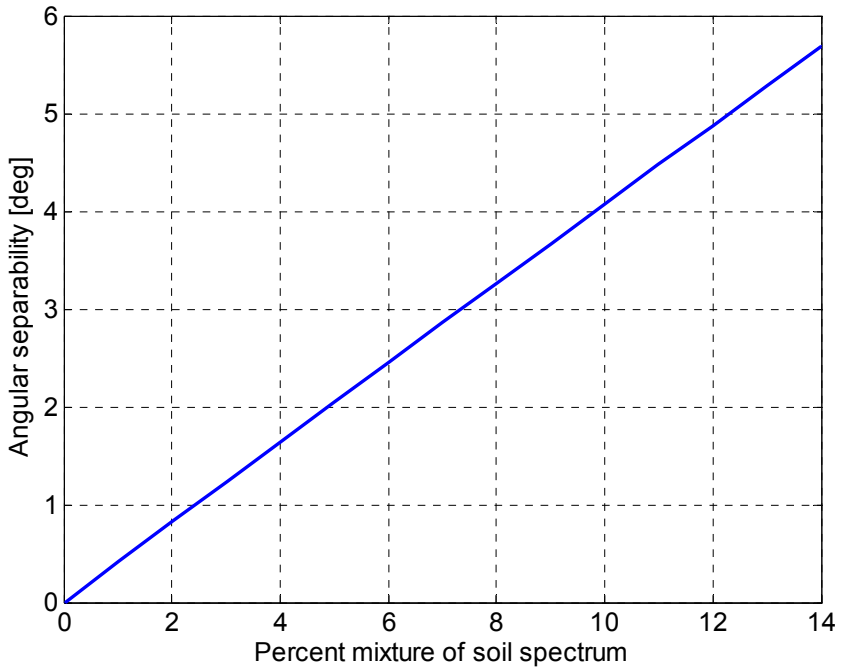

Figure 34. Within-class angular separation for Aspen leaf spectrum mixed with a soil spectrum.

The experiments conducted on materials identification with hyperspectral data are not conclusive due to the lack of sufficient within-class data. However, they do suggest that the discrimination of vegetation species is feasible with hyperspectral data. Data collections should be conducted to acquire several instances of each vegetation species of interest. Also, the calibration errors of the proposed atmospheric measurement and characterization device should be included in the analysis.

System Design Issues

In this section we discuss some system design issues such as spectral sensor configurations, companion sensors, sensor resolution requirements, and methodologies for nighttime operation.

Spectral and Companion Sensor Configurations

Four spectral sensor system designs are listed in order of increasing complexity and capability. Salient features of the designs are included such as complementary sensors, complementary image processing techniques, and distance/scale measurement issues.

- **#1: One CIR camera**
  - Broad feature multispectral analysis in conjunction with spatial texture analysis for materials identification
  - Spatial texture analysis handles the brunt of materials identification
  - Multispectral analysis in 3-4 bands facilitates object segmentation and broad categorization of materials
  - No moving parts
  - Daytime operation only
- **#2: Two CIR cameras, with one or more spectral bands in common.**
  - Crucial distance and scale information derived from stereoscopic pair
  - Requires at least one band in common for stereo fusion
  - Other bands need not be in common to gain wavelength diversity
  - Spatial texture analysis required for materials identification.
  - Multispectral analysis in 4-7 bands facilitates object segmentation and broad categorization of materials
  - No moving parts
  - Daytime operation only
- **#3: One RGB camera and a laser radar operating at ~0.83μm**
  - Distance and scale information derived from laser range image
  - RGB image combined with laser reflectance image to obtain CIR capability
  - There may be calibration problems in fusing RGB camera image with laser reflectance image. Needs to be researched.
  - Spatial texture analysis required for materials identification
  - RGB camera and IR laser are complementary sensors
  - Laser radar may require mechanical scanning
  - Day/night ranging and imaging, daytime materials classification

- **#4: Hyperspectral sensor, atmospheric calibration device, laser radar**
  - Atmospheric calibration device can be built to achieve 10% accuracy
  - Hyperspectral sensor for materials identification
  - Laser radar for distance and scale information
  - Spatial texture analysis still useful
  - Day/night ranging and imaging, daytime materials classification

Sensor Resolution and Field of View

A good reference point for determining the required sensor resolution is to consider materials identification through reflectance spectroscopy of a tree trunk. In order to identify a tree of some minimum trunk diameter, there should be at least three pixels across the trunk at some specified maximum range. For example, if we wish to identify a tree with a trunk diameter of 6" at a range of 50 ft., the trunk would occupy 0.573 degrees within the field of view. In order to achieve a total field of view of 60 degrees, the imaging sensor would need 104 pixels in the horizontal dimension. If the same tree trunk were at a range of 100 ft., the trunk would occupy 0.287 degrees within the field of view. In this case, the sensor would need 210 pixels in the horizontal dimension to span a 60-degree field of view.

Nighttime Operation

Nighttime operation poses an interesting challenge for materials identification. Reflectance spectroscopy for remote sensing usually relies on the presence of solar irradiance, which means that it is daytime-only. Thermal imaging in the TIR band relies on self-emission of materials, and is usually done at night to minimize contributions from reflectance. However, the emissivity function that determines the spectral character of the thermal emission can vary drastically over the surface of a plant. Consequently, TIR has proved to be unreliable for materials identification. Thus we are forced to consider ways to achieve materials identification through reflectance spectroscopy, which requires some sort of illumination source.

The simplest approach would be to utilize active illumination, either narrowband or broadband. Narrowband sources include laser diodes and traditional LEDs. A company called Luxeon manufacturers half-Watt LEDs that are approximately 25% efficient. They are available at the following wavelengths: 0.532, 0.570, 0.590, 0.610, 0.620, and 0.630μm. A company called AND corporation manufacturers an LED that operates at a wavelength of 0.8μm. One could consider sequencing LEDs of different wavelengths in time and utilizing a single-channel camera with broadband sensitivity. The result would be an active multispectral nighttime system with no moving parts.

Broadband sources include ordinary light bulbs, flash technology, and perhaps the more recent LED technology that utilizes an exciplex of blue-emitting organic molecules to produce broadband light [20].

An interesting alternative would be to utilize ambient nighttime illumination in the form of moonlight or starlight. Gen. III image intensifiers have usable response over a wavelength range of at least 0.5μm to 0.8μm. This response range is sufficient to support CIR multispectral processing. However, filters would have to be introduced to split the received light into bands. This would reduce the number of photons received per unit time at the sensor. This means that substantial integration times might be required to obtain sufficient light to perform materials identification.

A small amount of active illumination, perhaps using LEDs at specific wavelengths, could be used in conjunction with the image intensifier to reduce integration times and eliminate the need for optical filters at the receiver.

Finally, a multispectral laser radar could be developed for day/night CIR spectral analysis using laser diodes that are alternately pulsed at the desired frequencies.

Conclusions

A number of system concepts have been presented for using multispectral and hyperspectral sensing for materials identification to facilitate autonomous vehicle navigation. Potential advantages of materials identification include recognizing and avoiding plant species that tend to snag small robotic vehicles, avoiding hidden water hazards by recognizing plant species that grow at water's edge, and exploiting potential paths below tree species that tend to suppress undergrowth. There may also be utility in identifying road paving materials for road following.

The simplest concepts utilize CIR sensors to obtain multispectral data at a small number of wavelengths in the VIS and NIR bands. Materials can be categorized to some extent using three wavelengths in the visible and one wavelength in the NIR.

A number of metrics have been reported in the literature for distinguishing various characteristics of vegetation. The most common metric is the normalized difference vegetation index (NDVI). The NDVI is computed from reflectance measurements at visible red and NIR wavelengths using CIR, multispectral, or hyperspectral data. A strong positive NDVI value indicates the presence of photosynthetic plant material and can separate such material from a variety of other materials. Nonphotosynthetic or senesced plants exhibit lower NDVI values due to absent or reduced chlorophyll absorption in the visible spectral range, and are difficult to distinguish from other material classes. Other normalized difference indices include ones that compare reflectance in the green to red region (NDGR), and the blue to red region (NDBR). The NDGR metric can be used to separate leaves and needles from limbs and bark among photosynthetic vegetation. The NDBR metric can be used for separating paving materials from roadside materials for on-road navigation.

CIR sensing can only separate materials into broad categories. However, when spectral analysis is used in conjunction with texture analysis, detailed materials identification can be performed. For example, texture analysis of CIR data can identify plant species by their shape and structure. Spectral analysis of CIR data can also facilitate object segmentation by separating the boundaries of photosynthetic vegetation from background materials.

Object segmentation is perhaps the most difficult task. Range and scale information obtained by either stereoscopic video sensors or by laser radar is helpful if not essential for robust segmentation, and for determining navigability in general.

Multispectral sensors that utilize 5-20 wavelengths can do a better job than CIR sensors at categorizing materials into broad categories. An example was shown using six wavelengths to separate all vegetation from virtually all other materials. Additional complexity is involved because the wavelengths were spread across the visible, NIR, and SWIR bands. Also, some of the features were narrowband, requiring finespectral sensing. Inexpensive silicon-based sensors can measure reflectance in the visible and NIR up to about 1μm. Beyond that wavelength, other sensor materials are required, and the sensors become more expensive.

Hyperspectral sensors operating in the 0.4μm to 2.4μm wavelength range, demonstrate the potential to classify individual vegetation species. Additional data would be required to determine the bounds of within-class variations. Techniques were demonstrated for measuring reflectance properties in the presence of atmospheric variation. Atmospheric calibration was proposed in the form of a small device placed on the robotic vehicle that measures atmospheric aerosols and columnar water vapor. Such a device could measure atmospheric conditions with no more than 10% error. This might permit the utilization of standard laboratory reflectance spectra as exemplars for materials classification.

Finally, some system design issues were addressed including sensor resolution, sensor configurations with and without complementary sensors, and day/night operation.

References

[1] Schowengerdt, R. A., *Remote Sensing Models and Methods for Image Processing,* Second Edition, Academic Press, 1997

[2] Smith, J. L., Sandia National laboratories, personal communication.

[3] Vermote, E. et. al, 6S - *Second Simulation of Satellite Signal in the Solar Spectrum* Atmospheric modeling code, Laboratoire d'Optique Atmospherique, Universite des Sciences et Technologies de Lille, 59655 Villeneuve d'Ascq Cedex - France, E.C.M.W.F. Reading - England, and Code 923 / GIMMS group, GSFC/NASA, Greenbelt, MD 20771 - USA

[4] Clark, R. N., *Spectroscopy of Rocks and Minerals, and Principles of Spectroscopy*, Derived from Chapter 1 in: Manual of Remote Sensing, John Wiley and Sons, Inc. 1999.

[5] Clark, R.N., G.A. Swayze, A.J. Gallagher, T.V.V. King, and W.M. Calvin, *The U. S. Geological Survey, Digital Spectral Library: Version 1: 0.2 to 3.0*, 1993.

[6] Elvidge, C. D., *Visible and infrared reflectance characteristics of dry plant materials*, Int. J. of Remote Sensing, v. 11, no. 10, p. 1775 – 1795, 1990.

[7] Grove, C. I., Hook, S. J., and Paylor, E. D., *Laboratory reflectance spectra for 160 minerals 0.4 - 2.5 micrometers*: JPL Publication 92-2, Jet Propulsion Laboratory, Pasadena, CA., 1992.

[8] Korb, A. R., Dybwad, P., Wadsworth, W., and Salisbury, J. W., *Portable FTIR spectrometer for field measurements of radiance and emissivity*: Applied Optics, v. 35, p. 1679-1692, 1996.

[9] Salisbury, J. W., D'Aria, D. M., and Jarosevich, E., *Midinfrared (2.5-13.5 micrometers) reflectance spectra of powdered stony meteorites*: *Icarus*, v. 92, p. 280-297, 1991a.

[10] Salisbury, J. W., Wald, A., and D'Aria, D. M., *Thermal-infrared remote sensing and Kirchhoff's law 1. Laboratory measurements*: Jour. of Geophysical Research, v. 99, p. 11,897-11,911, 1994.

[11] Salisbury, J. W., Walter, L. S., Vergo, N., and D'Aria, D. M., Infrared (2.1-25 micrometers) Spectra of Minerals: Johns Hopkins University Press, 294 pp., 1991b.

[12] Hunt, F., NEF 9.1 Users Guide, http://www.math.nist.gov.

[13] Vane, G. and Goetz, A., *Terrestrial Imaging Spectroscopy, Remote Sensing of the Development Environment,* 24(1): 1-29, 1988.

[14] Kokaly, R. F. and Clark, R. N., *Spectroscopic Determination of Leaf Biochemistry Using Band-Depth Analysis of Absorption Features and Stepwise Linear Regression*, Remote Sensing Environment, Vol. 67, pp. 267-287, 1999.

[15] DeSouza, G. N. and Kak, A. C., *Vision for Mobile Robot Navigation: A Survey*, IEEE Trans. on Pattern Analysis and Machine Intelligence, 24(2): 237-267, 2002.

[16] Landsat 7 ETM+ bands obtained from NASA's Landsat website: http://www.geo.arc.nasa.gov/sge/landsat/landsat.htm.

[17] Harrison, L., Michalsky, J. and Bernt, J., *Automated multi-filter rotating shadow-band radiometer: an instrument for optical depth and radiation measurements*, Appl. Opt., 33(22), 1994.

[18] http://uvb.nrel.colostate.edu/UVB/ubv_instruments_mfrsr_frame.html.

[19] Clark, R. N. and Roush, T. L., *Reflectance spectroscopy: Quantitative analysis techniques for remote sensing applications*, Journal of Geophysical Research, **89**: 6239-6340, 1984.

[20] Thompson, J. et al, *White light emission from blends of blue-emitting organic molecules: A general route to the white organic light-emitting diode?* Applied Physics Letters, Vol. 79, No. 5, July 2001.

DISTRIBUTION:

1	MS	0844	W. J. Bow, 15352
1		0844	M. M. Moya, 15352
1		0844	B. K. Bray, 15352
1		0844	J. A. Richards, 15352
8		0844	R. J. Fogler, 15352
3		1125	J. J. Harrington 15252
1		0570	J. L. Smith 5712
1		9018	Central Technical Files, 8945-1
2		0899	Technical Library, 9616
1		0612	Review & Approval Desk, 9612 For DOE/OSTI